NUMERICAL SIMULATION AND STRUCTURAL OPTIMIZATION OF COMPOSITE RIGID FRAME BRIDGE

A Thesis
Submitted to the Graduate Faculty
of the
North Dakota State University
of Agriculture and Applied Science

By

Yanmei Xie

In Partial Fulfillment of the Requirements
for the Degree of
MASTER OF SCIENCE

Major Department:
Construction Management and Engineering

September 2017

Fargo, North Dakota

North Dakota State University
Graduate School

Title

NUMERICAL SIMULATION AND STRUCTURAL OPTIMIZATION OF COMPOSITE RIGID FRAME BRIDGE

By

Yanmei Xie

The Supervisory Committee certifies that this ***disquisition*** complies with North Dakota State University's regulations and meets the accepted standards for the degree of

MASTER OF SCIENCE

SUPERVISORY COMMITTEE:

Dr. Huojun Yang
Chair

Dr. Todd L. Sirotiak

Dr. Mike Christens

Approved:

11/1/2017
Date

Dr. Jerry Gao
Department Chair

ABSTRACT

A composite rigid frame bridge replaces a certain portion of the concrete middle span of a bridge with a section of the steel girder. While the steel span improves the bending moment distribution of the rigid frame structure, it increases the stress level of certain cross-sections of the girder. There is little research reporting the effects of the addition of the steel span on the layout and structural design. This research studies the influence of the steel span on the structural behavior of the rigid frame bridge and conducts the structural optimization regarding the steel span ratio, curve order of the girder's bottom line, and depth-to-span ratio using the bending strain energy as the objective function. Finally, this study develops the computer program for structural analysis of composite rigid frame bridge structure using MATLAB, which can be used for advanced structural optimization.

ACKNOWLEDGEMENTS

First, I would like to thank my academic advisor Dr. Huojun Yang for his academic guidance and support during my study. Also, I would like to thank my committee members: Dr. Todd L. Sirotiak from Construction Management and Engineering Department, and Dr. Mike Christens from Architecture and Landscape Architecture.

Furthermore, I would like to thank the Department of Construction Management and Engineering and College of Engineering at North Dakota State University for financial support during this research and my master program.

Finally, thanks for all the graduate students in Department of Construction Management and Engineering: Wanting Zhang, Dalu Zhang, Yuhan Jiang, Joseph Membah, etc., who helped the author during her work to complete this study. I would like to extend my gratitude to all my families in China who kept caring and supporting during my progress.

DEDICATION

I dedicate this work to my dear husband Zhiming Zhang for his endless support and understanding.

Final dedication to my dear parents and siblings for their deep concern and caring.

TABLE OF CONTENTS

ABSTRACT iii

ACKNOWLEDGEMENTS iv

DEDICATION v

LIST OF TABLES ix

LIST OF FIGURES x

1. INTRODUCTION 1

1.1. Composite Rigid Frame Bridge 1

1.2. Structural Optimization 2

1.3. Problem Statement and Research Objectives 3

1.4. Thesis Organization 4

2. FINITE ELEMENT MODEL DEVELOPMENT 5

2.1. Case Study 5

2.2. Finite Element Model Development 6

3. STEEL SPAN RATIO: PARAMETRIC ANALYSIS AND OPTIMIZATION 7

3.1. Parametric Analysis on Steel Span Ratio 7

3.1.1. Bending moments 7

3.1.2. Stresses 8

3.1.3. Deformation 10

3.1.4. Bending strain energy 11

3.2. Optimization on Steel Span Ratio 12

3.2.1. Optimization principle 12

3.2.2. The structural optimization 12

4. CURVE ORDER: PARAMETRIC ANALYSIS AND OPTIMIZATION 16

4.1. Parametric Analysis on Curve Order 16

4.1.1. Bending moments 16
4.1.2. Stresses 17
4.1.3. Deformation 20
4.1.4. Bending strain energy 22
4.2. Optimization on Curve Order 22
5. MIDSPAN DEPTH-TO-SPAN RATIO: PARAMETRIC ANALYSIS AND OPTIMIZATION 23
5.1. Parametric Analysis on Depth-to-Span Ratio 25
5.1.1. Bending moments 25
5.1.2. Stresses 27
5.1.3. Deformations 30
5.1.4. Bending strain energy 31
5.2. Optimization on Midspan Depth-to-Span Ratio 32
6. SUPPORT DEPTH-TO-SPAN RATIO: PARAMETRIC ANALYSIS AND OPTIMIZATION 33
6.1. Parametric Analysis on Depth-to-Span Ratio 33
6.1.1. Bending moments 33
6.1.2. Stresses 34
6.1.3. Deformations 36
6.1.4. Bending strain energy 37
6.2. Optimization on Support Depth-to-Span Ratio 38
7. COMPUTER PROGRAM DEVELOPMENT FOR MATRIX STIFFNESS STRUCTURAL ANALYSIS 39
7.1. Implementation of Matrix Stiffness Method 39
7.1.1. Structural discretization 39
7.1.2. Degree of freedom 40

7.1.3. Element stiffness matrix 40
7.1.4. Coordinate systems 41
7.1.5. Global stiffness matrix 41
7.1.6. Load assembly 45
7.1.7. Problem solving and internal force and reaction calculation 45
7.2. Program Development and Validation 47
7.2.1. Program development 47
7.2.2. Program validation 48
8. CONCLUSIONS AND FUTURE WORK 50
REFERENCES 52
APPENDIX. SCRIPTS 55

LIST OF TABLES

Table Page

1. Bending Moment at Steel Span Ratio of 0.2 - 0.8 (Unit: kN.m). 8

2. Stresses at the Top Edge at Different Steel Span Ratios (Unit: MPa). 9

3. Stresses at the Bottom Edge at Different Steel Span Ratios (Unit: MPa). 10

4. Deformation at Different Steel Span Ratios (Unit: cm)..... 11

5. Bending Strain Energy at Different Steel Span Ratios (Unit: kJ)..... 11

6. Bending Moments at Different Curve Orders (Unit: kN.m). 17

7. Stresses at the Top Edge at Different Curve Orders (Unit: MPa)..... 18

8. Stresses at the Bottom Edge at Different Curve Orders (Unit: MPa). 19

9. Deformations at Different Curve Orders (Unit: cm)..... 21

10. Bending Strain Energy at Different Curve Orders (Unit: kJ). 22

11. Examples of Depth-to-Span Ratio of Large-Span Rigid Frame Bridges. 24

12. Bending Moments at Different Midspan Depth-to-Span Ratio (Unit: kN.m). 26

13. Stresses at the Top Edge at Different Midspan Depth-to-Span Ratios (Unit: MPa). 28

14. Stresses at the Bottom Edge at Different Midspan Depth-to-Span Ratios (Unit: MPa). 29

15. Deformations at Different Midspan Depth-to-Span Ratios (Unit: cm). 30

16. Bending Strain Energy at Different Midspan Depth-to-Span Ratios (Unit: kJ). 31

17. Bending Moments at Different Depth-to-Span Ratios (Unit: kN.m)..... 33

18. Stresses at the Top Edge at Different Depth-to-Span Ratios (Unit: MPa). 35

19. Stresses at the Bottom Edge at Different Depth-to-Span Ratios (Unit: MPa). 36

20. Deformations at Different Depth-to-Span Ratios (Unit: cm). 37

21. Bending Strain Energy at Different Depth-to-Span Ratios (Unit: kJ). 38

22. Comparison of Bending Moments from Finite Element Analysis and Computer Program (kN.m) 49

LIST OF FIGURES

Figure Page

1. Bending Moment Distribution of Composite Bridge Girder. 1

2. The Layout of Oujiang Bridge (Unit: cm) 5

3. The Bridge Finite Element Model. 6

4. Sum of Bending Moment at Different Span Ratios (Unit: kN.m). 13

5. Sum of Top Edge Stress at Different Span Ratios (Unit: MPa). 14

6. Sum of Bottom Edge Stress at Different Span Ratios (Unit: MPa). 14

7. Sum of Bridge Deformation at Different Span Ratios (Unit: cm). 15

8. Bending Moments at Different Curve Orders. 17

9. Stress at the Top Edge of Sections at Different Curve Orders. 19

10. Stress at the Bottom Edge at Different Curve Orders. 20

11. Deformation at Different Curve Orders. 21

12. Bending Strain Energy at Different Curve Orders. 22

13. Bending Moment at Different Depth-to-Span Ratios. 26

14. Stress at the Top Edge at Different Midspan Depth-to-Span Ratio. 28

15. Stress at the Bottom Edge at Different Depth-to-Span Ratios. 29

16. Deformation at Different Depth-to-Span Ratios. 31

17. Relative Bending Strain Energy at Different Depth-to-Span Ratios. 32

18. Bending Moment at Different Depth-to-Span Ratios. 34

19. Stress at the Top Edge at Different Depth-to-Span Ratios. 35

20. Stress at the Bottom Edge at Different Depth-to-Span Ratios. 36

21. Deformation at Different Support Depth-to-Span Ratios. 37

22. Bending Strain Energy at Different Support Depth-to-Span Ratios. 38

23. Degree of Freedom of Frame Element 40

24. Coordinate Systems for Structural Analysis. 41

25. Example Frame Structure and its Discretization and Coordinate System. 43

1. INTRODUCTION

1.1. Composite Rigid Frame Bridge

A continuous rigid frame bridge has a rigid connection between the girders and piers, making them work together under traffic loads. The fact that the piers bear both axial force as well as bending moment decreases the positive bending moment at the midspan of the girder and thus reduces the girder depth [1-3]. A composite rigid frame bridge, composed of steel-concrete girder and reinforced concrete piers, has a lower bridge weight and more reasonable internal force distribution compared to traditional rigid frame bridge. Sharing the benefits of both a rigid frame bridge and a composite structure, the composite rigid frame bridge has advantages over other bridge types with respect to the spanning capability and material and construction costs [4-7]. Figure 1 shows the comparison of the bending moment distribution of the concrete rigid frame bridge with the composite rigid frame bridge. The overall design of the composite rigid frame bridge generally follows the same procedures of the steel or concrete rigid frame bridge design, except the determination of the position of the steel-concrete intersection point with a given main span, i.e. the portion of steel segment in the midspan [8-11].

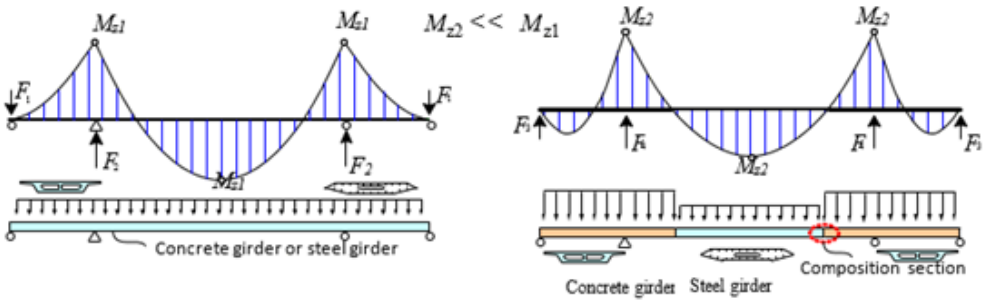

Figure 1. Bending Moment Distribution of Composite Bridge Girder.

1.2. Structural Optimization

The main importance of structure engineering is to design a safe and economical structure. Economy in design can be achieved through an optimization procedure. The purpose of structural optimization is to find the most efficient structure, which satisfies the chosen criteria [12] . Wild et al. [13] defined the optimum design "the best feasible design according to a preselected quantitative measure of effectiveness". Researchers have implemented and developed many optimization methods. Genetic Algorithm (GA) has been used for the optimization of concrete structures. Lute et al. [14] combined a Genetic Algorithm (GA) and support vector machine (SVM) to carry out the optimization design of cable-stayed bridge structures. Cheng et al. [15] proposed an algorithm integrating the concepts of the GA and the finite element method, which used the weight of the structure, strength (stress), and serviceability (deflection) constraints as the objective function. Hassan et al. [16] developed a design optimization technique combined finite element method, B-spline curves, and Genetic Algorithm, which was tested and assessed by application to a practical sized cable-stayed bridge. Martins et al. [17] and Baldomir et al. [18] applied a gradient based approach to optimize stay cabled bridges, however, they used different software. Martins et al. [17] used the software MATLAB to optimize the cable forces, and Baldomir et al. [18] used the software Abaqus to model the structure to optimize the cross-sectional areas of a cable-stayed bridge in the design phase. Kusano et al. [19] investigated the reliability based design optimization of long-span bridges with consideration to flutter. Based on the Simulated Annealing (SA), Martí et al. [20] developed an optimization algorithm to minimize the cost of prestressed concrete bridges. The study of Martínez et al. [21] applied the Ant Colony Optimization (ACO) for optimum design of tall bridge piers. Even though there are many optimum design methods, they have the similar characteristics: (1) preassigned parameters, (2) design variables, (3) load conditions, (4)

failure modes, and (5) objective function, also termed merit or criterion function [22]. An important procedure of structural optimization is the determination of objective function. In the optimization method, the optimization of certain objective functions may either be related to structural efficiency or economy.

Sensitivity can be defined as a response derivative with regards to a design variable, that is, a structural property with a potential for change. This derivative can be understood as the expected change in the response when the considered design variable is perturbed [23-25]. Sensitivity is an important part to help the designer avoid unreasonable design results by following a guided design process. There are several publications about the application of sensitivity found, which gained confidence to be applied to the bridge design [26-29]. The fundamental principle of a composite rigid frame bridge design is to balance the weight and traffic load from the midspan with the concrete side span which has more weight and stiffness. The maximum internal force or stress itself can't reflect the performance of a bridge design plan due to the fact that an optimization plan may reduce the responses of a cross section while increase the responses elsewhere. Bridge's strain energy comprehensively reflects the influence of bending moments considering the members' flexural stiffness. It has been widely used as the objective function for structural optimization [30-36].For girder type bridge, e.g., rigid frame bridge, the strain energy from axial forces is very small compared with the bending strain energy. In this case, the bending strain energy itself is sufficient for the structural optimization purpose.

1.3. Problem Statement and Research Objectives

Majority of optimization applications are for steel structures and very few for composite and concrete structures[12]. The literature review indicates that the state-of-the-art of research on

composite rigid frame bridge lacks a comprehensive structural optimization considering the contributions to the bridge's performance from different structural parameters.

To solve this challenge, the main objective of this dissertation is to develop a systematic method for structural optimization of composite rigid frame bridge. The main tasks in this study include:

1) Develop a finite element model using a commercial software MIDAS CIVIL;
2) Conduct parametric analysis on structural parameters of bridge including steel span ratio, curve order of bottom line, and depth-to-span ratio;
3) Optimize the bridge structure based on the contributions of structural parameters to the bridge performance;
4) Develop and validate a computer program for composite rigid frame bridge modelling and analysis using MATLAB.

1.4. Thesis Organization

Based on the specific tasks aligned to achieve the main objective of this study above, this thesis is divided into seven chapters as follows: Chapter 2 develops the finite element model for structural analysis and optimization; Chapters 3, 4, 5, and 6 conduct the parametric analysis and optimization on steel span ratio, curve order of bottom line, and depth-to-span ratio of composite rigid frame bridge, respectively; Chapter 7 develops the computer program for structural analysis using MATLAB and validates the program by comparison with a commercial software. Chapter 8 presents conclusions and recommended future work.

2. FINITE ELEMENT MODEL DEVELOPMENT

2.1. Case Study

This section introduces a case study to illustrate a detailed implementation using the structural optimization method both theoretically and numerically. This case study takes the Oujiang Bridge as an example for structural optimization. The Oujiang Bridge is part of the Zhuyong Highway and the second steel-concrete composite rigid frame bridge in China. It has three spans with a midspan of 200m and two side spans of 84m, respectively. Figure 2 shows the layout of the Oujiang Bridge. The center 80m section of the 200m midspan is steel girder with the rest of the bridge made of concrete. The depth of the concrete girder is 9.0m at the inner supports and 3.5m at the intersection, and the steel girder has the same depth with the concrete girder at the intersection for geometry compatibility and consistence. The top and bottom surfaces of the bottom flange follow two parabolas of 1.6 order, as are shown in Equations 1 and 2, respectively.

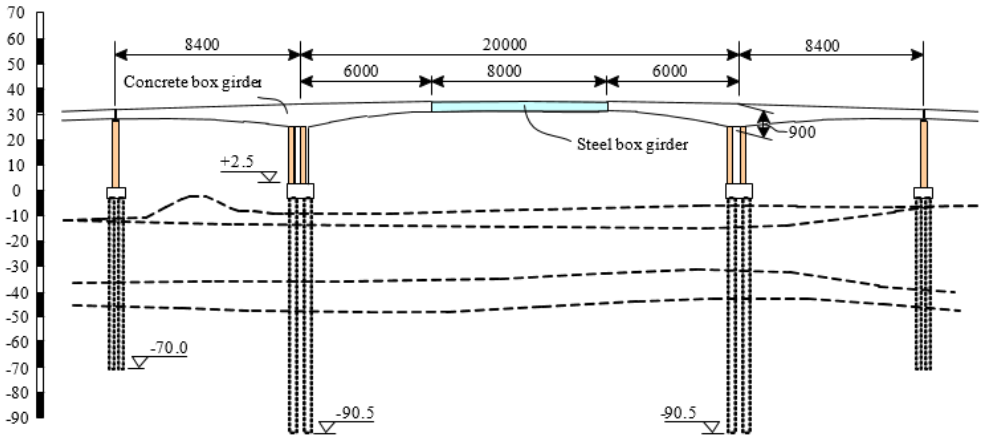

Figure 2. The Layout of Oujiang Bridge (Unit: cm)

$$y^{t} = 0.000478982x^{1.6} \quad (1)$$

$$y^{b} = 0.000553684x^{1.6} \quad (2)$$

2.2. Finite Element Model Development

Numerical analysis such as finite element analysis plays an important role for structure design and optimization. Validated finite element model can be used for structural parametric analysis and further optimization. This study develops the beam-element numerical model of the composite rigid frame bridge using MIDAS/CIVIL 2016 and validates the numerical model with the analytical model developed in 3.1. The finite element model also considers the cantilever-construction stages including the concrete casting and steel girder erection. As to the boundary conditions, the bottom ends of the piers are fixed and the beam is simply supported. Figure 3 illustrates the finite element model of the bridge.

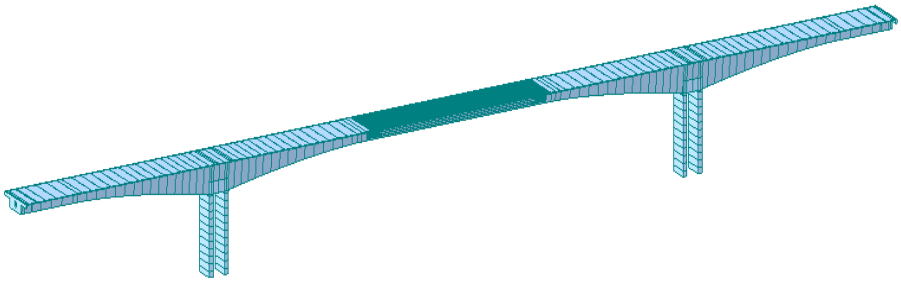

Figure 3. The Bridge Finite Element Model.

3. STEEL SPAN RATIO: PARAMETRIC ANALYSIS AND OPTIMIZATION

3.1. Parametric Analysis on Steel Span Ratio

This study conducts the structural parametric analysis taking the steel span ratio as the variable using the finite element model that is developed and validated in **3.2**. In the parametric analysis, the steel span ratio ranges from 0.2 to 0.8 at an interval of 0.05, ending up with 13 cases. Considering that the dead load takes a large part compared with live load for large-span bridge, the study uses dead load for parametric analysis and structural optimization. For each case, the bridge responses including the bending moment, stress, and displacement of several important sections are extracted from the finite element analysis results. In each case, the bending strain energy is calculated by Equation 2. Coefficient of variation (C.V.) is used to measure the amount of variability relative to the mean. Coefficients of variation of different cases are comparable as the influence from the unit difference and mean value magnitude are eliminated [37]. The expression of coefficient of variation is as shown in Equation 3,

$$\text{C.V.} = \frac{\sigma}{\mu} \times 100\% \tag{3}$$

where σ is the standard deviation, and μ is the mean value.

3.1.1. Bending moments

Table 1 lists the bending moments of the beam at different steel span ratios. The locations of cross sections for consideration and comparison include ¼, ½, and ¾ side span from the abutment support, the top of left pier and right pier, ¼ midspan from the right pier, the intersection of steel and concrete girders, and the center of midspan, considering the symmetricity of the bridge structure. The bending moment with the bottom of the section in tension is labeled as positive, and the moment with the top in tension as negative. As the steel span ratio increases, the bending moments of all the eight cross sections increase except that of the intersection location, which

decreases to a negative moment from a positive moment. The moments at the ¼ and ½ side spans also change directions. The bending moment magnitudes don't reach minimum at the same or close steel span ratio, indicating that the bending moment itself is not sufficient for structural optimization. The coefficient of variation reaches the maximum at the ½ side span and the second maximum at the intersection, which mean that the steel span ratio has largest influence on the bending moment distribution at these two locations.

Table 1. Bending Moment at Steel Span Ratio of 0.2 - 0.8 (Unit: kN.m).

Steel span ratio	¼ side span	½ side span	¾ side span	Left pier	Right pier	¼ midspan	Intersection	Center of midspan
0.2	-48752	-279682	-754166	-1400801	-1587499	-237100	46651	79218
0.25	-16447	-215622	-651348	-1263821	-1442163	-188412	32428	78623
0.3	10035	-162532	-564573	-1148905	-1328613	-154641	16528	83987
0.35	32576	-117314	-489427	-1047308	-1218547	-125658	-1695	89785
0.4	51422	-79889	-426066	-960580	-1117568	-103981	-23756	96372
0.45	67782	-47962	-371201	-883581	-1022386	-86940	-47877	103736
0.5	86447	-12430	-311509	-800311	-934798	-83529	-75656	112177
0.55	93707	1320	-285369	-759210	-859249	-56935	-108217	120274
0.6	104348	20446	-251163	-707191	-781317	-56578	-141602	132042
0.65	114105	38637	-221059	-660206	-714973	-45348	-179642	143630
0.7	125109	59221	-188644	-610591	-651762	-29973	-218351	159006
0.75	133655	75207	-164119	-570560	-602368	-18047	-265016	170932
0.8	142761	99551	-156743	-530097	-595087	-2932	-312956	186046
C.V., %	87.0	-245.5	-52.0	-31.6	-33.4	-75.7	-119.6	30.2

3.1.2. Stresses

Table 2 and Table 3 tabulate the bending stresses on the top and bottom edges of the cross sections at different steel span ratios, respectively. The positive stress in the charts indicates tension, while the negative stress indicates compression. All the stresses at the top edge decrease with the increase of the steel span ratio due to the monotonic increase of bending moments as shown in Table 1, except the stresses at the ¼ midspan and the intersecting cross sections. The top edge stress at the ¼ midspan cross section decreases smoothly before the steel span ratio

surpasses 0.5, when the ¼ midspan cross section becomes the concrete side of the intersecting cross section. At steel span ratios is 0.55, an abrupt increase happens due to the material and dimension change at this cross section. The top edge stress decreases smoothly after this sudden change. The top edge stress increases monotonically at the cross section of intersection due to the monotonic decrease of bending moment thereof as shown in Table 2. Correspondingly, the bottom edge stress shows opposite variation trend due to the sign difference. Consistent with that of the bending moment, C.V. of bending stresses reaches it first and second maximum at the ½ side span and the intersecting cross sections, respectively. The largest tension and compressive stress magnitudes both increase consistently with the steel span ratio. Furthermore, both of them happen at the center of midspan, which is located on the steel section of the composite rigid frame bridge with much larger strength than concrete. Additionally, other the stress magnitudes don't variate consistently with that of the midspan center. Therefore, the parametric analysis on bending stresses does not yield a steel span ratio that optimizes the stress level at all the critical locations.

Table 2. Stresses at the Top Edge at Different Steel Span Ratios (Unit: MPa).

Steel span ratio	¼ side span	½ side span	¾ side span	Left pier	Right pier	¼ midspan	Intersection	Center of midspan
0.2	2.28	8.93	15.50	11.20	12.60	8.75	-2.92	-45.00
0.25	0.82	7.26	13.70	10.10	11.10	7.36	-2.11	-46.80
0.3	-0.55	5.81	12.20	9.15	10.60	6.43	-1.21	-47.90
0.35	-1.85	4.50	10.90	8.33	9.70	5.60	-0.17	-48.60
0.4	-2.98	3.31	9.79	7.64	8.89	4.98	1.10	-55.00
0.45	-3.93	2.17	8.90	7.03	8.13	4.47	2.48	-59.00
0.5	-5.02	0.61	7.86	6.36	7.43	4.51	4.08	-63.70
0.55	-5.44	-0.09	7.69	6.03	6.83	32.45	5.96	-68.10
0.6	-6.06	-1.19	7.37	5.61	6.21	26.10	7.88	-74.50
0.65	-6.62	-2.25	7.26	5.24	5.68	19.85	10.10	-80.70
0.7	-7.26	-3.44	7.25	4.84	5.17	11.53	12.30	-89.00
0.75	-7.76	-4.37	7.83	4.52	4.78	5.29	15.00	-95.30
0.8	-8.29	-5.35	9.20	4.20	4.69	-2.79	17.80	-103.00
C.V., %	-83.6	372.5	27.8	32.0	33.1	95.6	125.3	-29.2

Table 3. Stresses at the Bottom Edge at Different Steel Span Ratios (Unit: MPa).

Steel span ratio	¼ side span	½ side span	¾ side span	Left pier	Right pier	¼ midspan	Intersection	Center of midspan
0.2	-3.44	-11.9	-18.6	-13.5	-15.3	-12.6	4.2	80.7
0.25	-1.28	-9.81	-16.5	-12.2	-19.8	-10.9	2.85	79.9
0.3	0.84	-8.01	-14.8	-11.1	-12.8	-9.91	1.32	85.3
0.35	2.98	-6.35	-13.3	-10.1	-11.8	-8.99	-0.42	91.3
0.4	4.87	-4.82	-12.1	-9.29	-10.8	-8.38	-2.53	98
0.45	6.42	-3.28	-11.1	-8.54	-9.88	-7.88	-4.83	106
0.5	8.19	-0.99	-9.97	-7.74	-9.04	-8.14	-7.47	114
0.55	8.88	0.1	-9.93	-7.35	-8.31	-76.55	-10.6	123
0.6	9.88	1.94	-9.75	-6.85	-7.56	-64.5	-13.7	135
0.65	10.8	3.66	-9.95	-6.39	-6.92	-52.1	-17.4	147
0.7	11.9	5.61	-10.5	-5.92	-6.31	-36	-21	163
0.75	12.7	7.13	-12.2	-5.53	-5.84	-23.4	-25.5	176
0.8	13.5	8.74	-14.83	-5.14	-5.80	-7.4	-30	192
C.V., %	82.7	-479.7	-22.7	-31.4	-41.1	-96.6	-116.3	30.7

3.1.3. Deformation

Table 4 tabulates the deformation of the bridge girder at different steel span ratios. Similar to the bending moment and stress, deformation demonstration various trends with the increase of steel span ratio, as is displayed in Figure 7. However, the coefficients of variation don’t show much difference at different sections.

Table 4. Deformation at Different Steel Span Ratios (Unit: cm).

Steel span ratio	¼ side span	½ side span	¾ side span	¼ midspan	Intersection	Center of midspan
0.2	-17.44	-9.27	-0.99	-21.75	-48.77	-21.06
0.25	-14.15	-7.94	-0.85	-19.94	-39.12	-22.23
0.3	-11.19	-8.17	-0.72	-18.20	-31.38	-24.60
0.35	-8.64	-5.84	-0.63	-16.70	-24.91	-26.90
0.4	-1.75	-5.25	-0.59	-15.41	-17.59	-29.52
0.45	-2.62	-4.80	-0.56	-14.17	-15.04	-32.30
0.5	-3.80	-3.99	-0.48	-13.88	-12.83	-35.67
0.55	-4.39	-4.35	-0.56	-14.98	-9.93	-38.98
0.6	-5.24	-4.18	-0.59	-17.27	-8.64	-44.46
0.65	-6.06	-4.71	-0.62	-19.96	-6.45	-50.28
0.7	-7.17	-5.92	-0.67	-24.67	-5.01	-59.15
0.75	-7.83	-6.89	-0.70	-28.69	-3.29	-66.41
0.8	-8.79	-8.19	-1.91	-34.97	-2.43	-76.79
C.V., %	-59.5	-29.2	-21.4	-31.0	-84.3	-43.8

3.1.4. Bending strain energy

Table 5 lists the bending strain energy at different steel span ratios calculated by Equation 2. The relative energy in the third row is calculated taking the minimum strain energy as the reference, which is also illustrated in Figure 8. The bending strain energy reaches the minimum value at a steel span ratio of 0.55, which means that the bending moment of the bridge reaches a reasonable distribution considering the stiffness variation along the bridge.

Table 5. Bending Strain Energy at Different Steel Span Ratios (Unit: kJ).

Steel span ratio	0.2	0.25	0.3	0.35	0.4	0.45	0.5	0.55	0.6	0.65	0.7	0.75	0.8
Bending strain energy (kJ)	11395	9138	7524	6279	5415	4758	4324	4105	4164	4307	5032	5399	6369
Relative energy	2.74	2.19	1.81	1.51	1.30	1.14	1.04	1.00	1.01	1.03	1.21	1.30	1.48

3.2. Optimization on Steel Span Ratio

3.2.1. Optimization principle

The fundamental principle of composite rigid frame bridge design is to balance the weight and traffic load from the midspan with the concrete side span with more weight and stiffness. The maximum internal force or stress itself can't reflect the perforce of a bridge design plan due to the fact that an optimization plan may reduce the responses of a cross section while increase the responses elsewhere. Bridge's bending strain energy comprehensively reflects the influence of bending moments considering the members' flexural stiffness. It has been widely used as the objective function for bridge structural optimization [30, 31]. Equation 1 is the expression of bending strain energy.

$$U_{\mathrm{b}} = \sum_{i} \int_{L_i} \frac{M_i^{\,2}(x)}{2(EI)_i} dx \tag{3}$$

where m is the total number of the elements, U_{b} is the bending strain energy, L_i is the length of the i^{th} element, E is the modulus of elasticity, I is the moment of inertia, and $M_i(x)$ is the magnitude of moment at the location x of the i^{th} element. The discrete expression of bending strain energy for numerical calculation is

$$U_{\mathrm{b}} = \sum_{i=1}^{m} \frac{L_i}{4(EI)_i} \left(M_{iL}^2 + M_{iR}^2 \right) \tag{4}$$

where $M_{i\mathrm{L}}$ and $M_{i\mathrm{R}}$ are the bending moment at the left and right end of the i^{th} element, respectively.

The bridge structural optimization in this study takes the steel span ratio of the midspan as the variable and the bending strain energy as the objective function.

3.2.2. The structural optimization

The parametric analysis in 3.1 indicates that a small value of steel span ratio leads to a significant bending moment and that a large value results in a large bending stress and a

considerable deformation. The compromise of bending moment, bending stress, and bridge deformation ends up with a moderate value of steel span ratio for structural optimization. The analysis on bending strain energy, a comprehensive evaluation of bridge's mechanical performance and economic benefits, concludes a steel span ratio of 0.55. Figures Figure 4- Figure 7 illustrate the sum of responses at the important sections at different span ratios. These figures demonstrate that the case with a span ratio of 0.55 has a relative low value of bending moment and deformation summation while a high level of stress summation. As the high stresses always happen on steel girder that has much higher strength than concrete, a span ratio of 0.55 is an acceptable result of structural optimization.

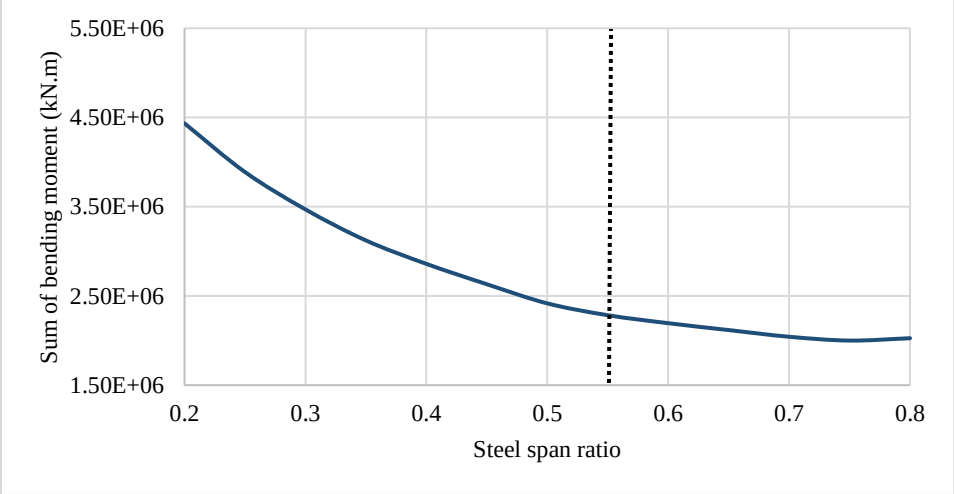

Figure 4. Sum of Bending Moment at Different Span Ratios (Unit: kN.m).

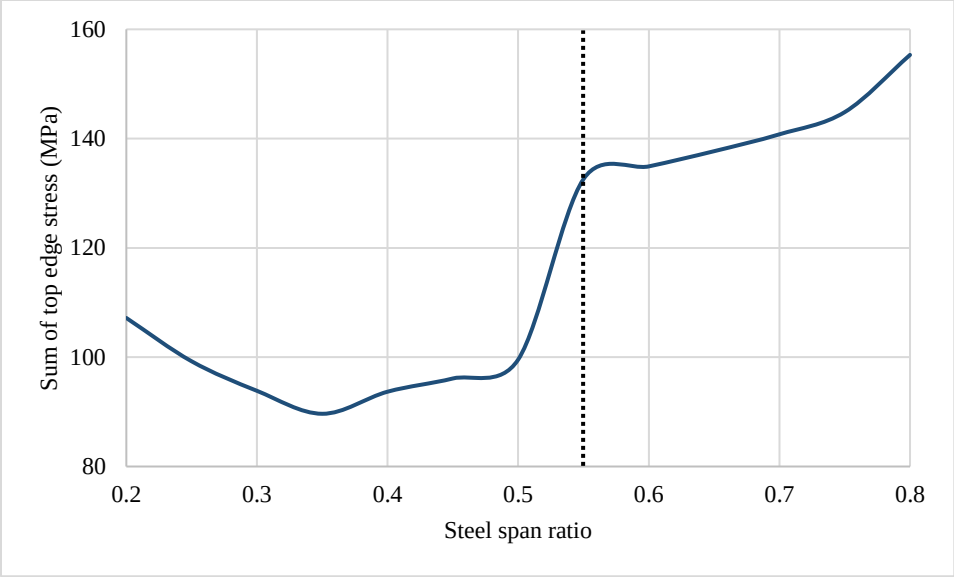

Figure 5. Sum of Top Edge Stress at Different Span Ratios (Unit: MPa).

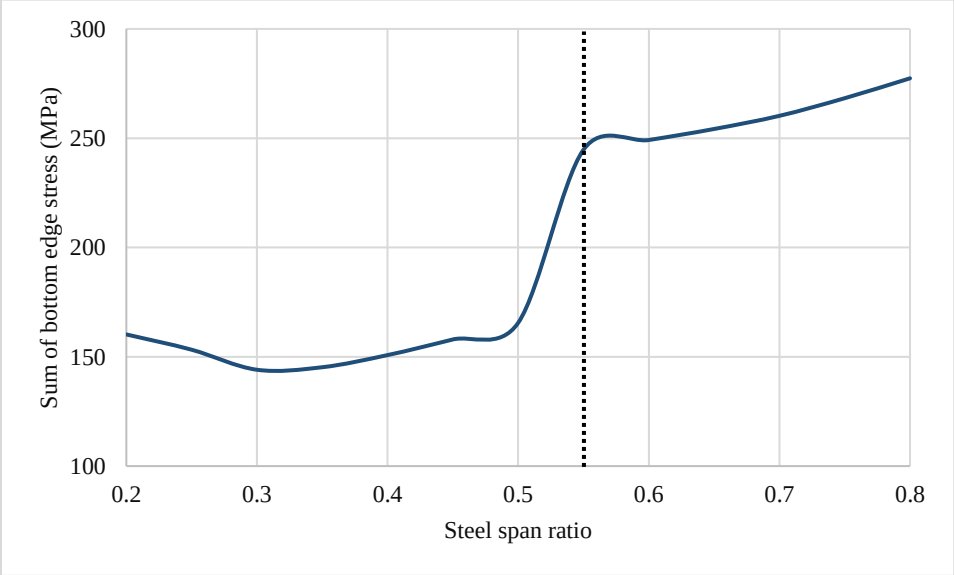

Figure 6. Sum of Bottom Edge Stress at Different Span Ratios (Unit: MPa).

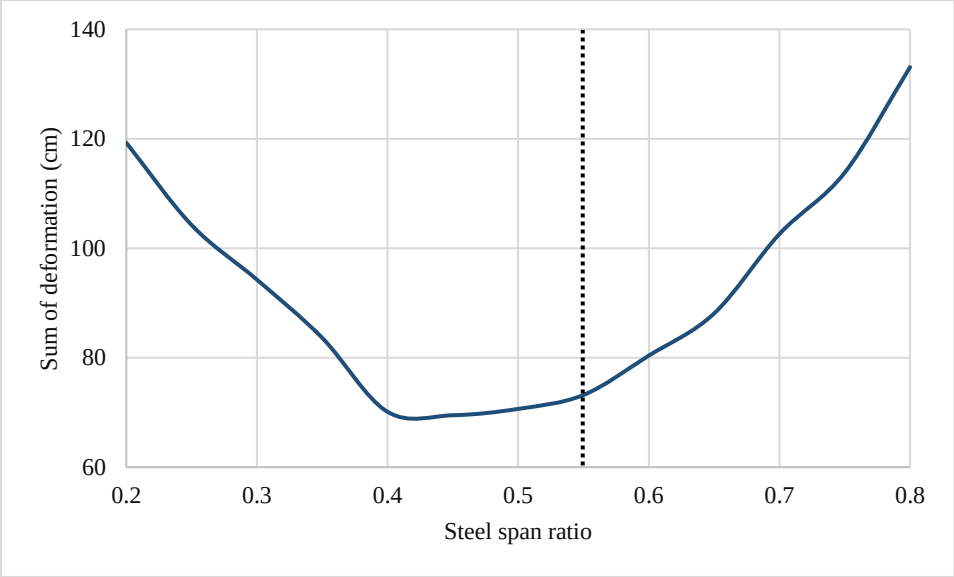

Figure 7. Sum of Bridge Deformation at Different Span Ratios (Unit: cm).

4. CURVE ORDER: PARAMETRIC ANALYSIS AND OPTIMIZATION

4.1. Parametric Analysis on Curve Order

This section conducts the parametric analysis on the order of the girder's bottom curve that ranges from 1.3 to 2. The indicators of bridge's performance include bending moments, stresses at the top and bottom edges of cross sections, deformations, and bending strain energy. The parametric analysis lays a foundation for structural optimization.

4.1.1. Bending moments

Table 6 and Figure 8 lists and illustrates the bending moments at the eight important cross sections at with the increase of curve orders. All of the moments are increasing with the curve orders in the direction of positive bending moments. The moment at the right pier has the largest increase of 87364KN.m. The coefficient of variation reaches the maximum at the steel-concrete intersection, i.e., 30.7%, which indicates that the bridge girder's curve order has the largest influence on the bending moment at the intersection.

Table 6. Bending Moments at Different Curve Orders (Unit: kN.m).

Curve order	¼ side span	½ side span	¾ side span	Left pier	Right pier	¼ midspan	Intersection	Center of midspan
1.3	77630	-32993	-372608	-919342	-1278044	-83369	10991	130742
1.35	77994	-31933	-368340	-910466	-1267978	-81509	12847	132601
1.4	78093	-31424	-365147	-903248	-1259302	-80254	14105	133866
1.45	78488	-30385	-361388	-895490	-1250618	-78447	15918	135682
1.5	78546	-29909	-358276	-888612	-1242770	-77233	17148	136919
1.55	79008	-28874	-355127	-882097	-1235628	-75491	18891	138663
1.6	79228	-28301	-352825	-877053	-1217204	-72995	19676	139509
1.65	79571	-27410	-349739	-870611	-1222886	-72681	21721	141501
1.7	79884	-26692	-347447	-865716	-1217063	-71322	23110	142894
1.75	80175	-25987	-345129	-860834	-1212188	-70046	24375	144161
1.8	80621	-25032	-342074	-854179	-1205256	-68353	26077	145868
1.85	80792	-24593	-340931	-851988	-1202706	-67518	26922	146715
1.9	81094	-23926	-339017	-847983	-1198448	-66317	28135	147930
1.95	81473	-23183	-337354	-844579	-1194353	-65120	29341	149133
2	81694	-22618	-335411	-840558	-1190680	-63989	30483	150283
C.V.	1.8%	-13.0%	-3.6%	-3.1%	-2.4%	-9.1%	30.7%	4.7%

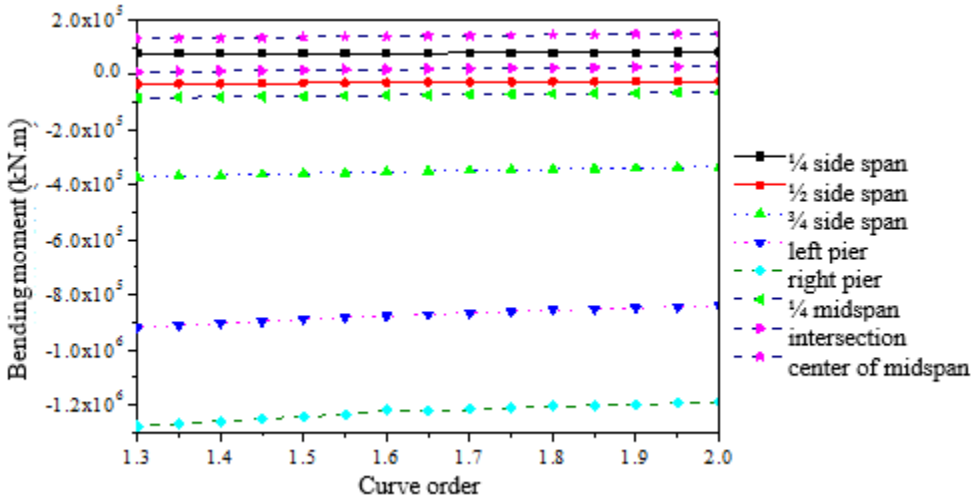

Figure 8. Bending Moments at Different Curve Orders.

4.1.2. Stresses

Table 7 tabulates the Stresses at the top edge of the important cross sections at different curve orders, which is also shown in Figure 9. It can be seen that the curve order has very limited

influence on the stresses at the top edge. The coefficients of variation are within 5% except that at the steel-concrete intersection where the variation of stress is less than 1 MPa. This indicates that the stress at the top edge of bridge girder needs not to be included for consideration during the structural optimization of curve order.

Table 8 and Figure 10 are the diagrams for stresses at the bottom edge at different curve orders. Similar to the stresses at the top edge the curve order has little influence on the stress at the bottom edge with all the coefficients of variation below 5%. Therefore, the stress at the bottom edge will not be considered for the curve order optimization.

Table 7. Stresses at the Top Edge at Different Curve Orders (Unit: MPa).

Curve order	¼ side span	½ side span	¾ side span	Left pier	Right pier	¼ midspan	Intersection	Center of midspan
1.3	-4.51	1.17	7.74	7.31	10.10	3.52	-0.60	-73.60
1.35	-4.53	1.16	7.75	7.24	10.10	3.50	-0.68	-74.60
1.4	-4.53	1.17	7.78	7.19	9.99	3.50	-0.73	-75.30
1.45	-4.56	1.15	7.80	7.12	9.92	3.47	-0.80	-76.20
1.5	-4.56	1.15	7.84	7.07	9.86	3.47	-0.85	-76.90
1.55	-4.59	1.13	7.87	7.02	9.80	3.44	-0.92	-77.80
1.6	-4.60	1.13	7.91	6.98	9.65	3.36	-0.96	-78.20
1.65	-4.62	1.12	7.95	6.93	9.70	3.39	-1.03	-79.30
1.7	-4.64	1.10	8.00	6.89	9.65	3.38	-1.09	-80.00
1.75	-4.65	1.09	8.04	6.85	9.61	3.33	-1.14	-80.70
1.8	-4.68	1.07	8.10	6.79	9.56	3.27	-1.21	-81.50
1.85	-4.69	1.06	8.15	6.78	9.54	3.26	-1.24	-82.00
1.9	-4.71	1.05	8.20	6.74	9.50	3.22	-1.29	-82.60
1.95	-4.73	1.02	8.26	6.72	9.47	3.19	-1.34	-83.30
2	-4.74	1.02	8.31	6.69	9.44	3.15	-1.39	-83.90
C.V.	-1.8%	5.0%	2.5%	3.0%	2.4%	3.9%	-26.8%	-4.4%

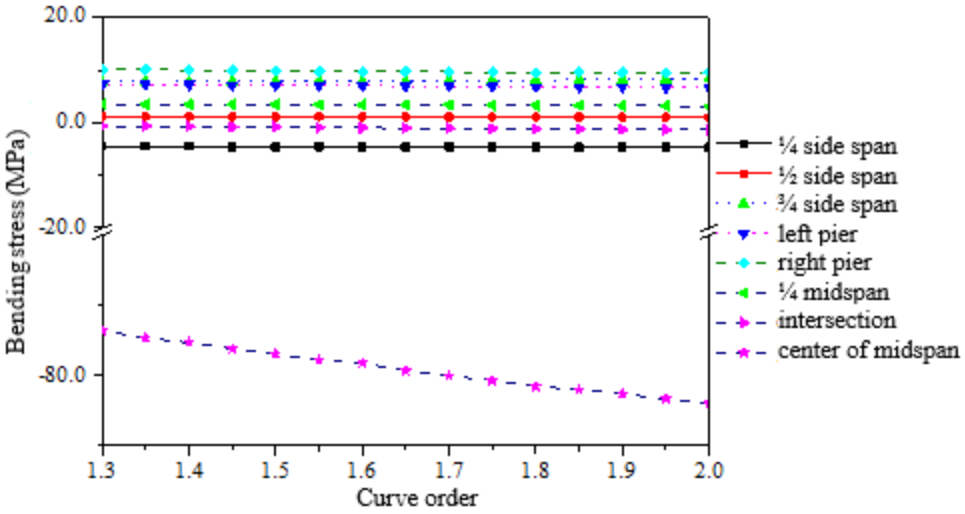

Figure 9. Stress at the Top Edge of Sections at Different Curve Orders.

Table 8. Stresses at the Bottom Edge at Different Curve Orders (Unit: MPa).

Curve order	¼ side span	½ side span	¾ side span	Left pier	Right pier	¼ midspan	Intersection	Center of midspan
1.3	7.35	-1.63	-9.19	-8.89	-12.40	-5.90	0.46	134
1.35	7.39	-1.64	-9.28	-8.80	-12.30	-5.95	0.57	136
1.4	7.40	-1.68	-9.39	-8.73	-12.20	-6.03	0.64	137
1.45	7.44	-1.68	-9.48	-8.66	-12.10	-6.06	0.74	139
1.5	7.44	-1.72	-9.57	-8.59	-12.00	-6.12	0.82	140
1.55	7.48	-1.71	-9.67	-8.53	-12.00	-6.11	0.91	142
1.6	7.51	-1.72	-9.76	-8.48	-11.80	-6.02	0.96	143
1.65	7.54	-1.72	-9.88	-8.42	-11.90	-6.12	1.07	145
1.7	7.57	-1.71	-9.98	-8.37	-11.80	-6.16	1.15	147
1.75	7.60	-1.70	-10.10	-8.32	-11.70	-6.09	1.23	148
1.8	7.64	-1.68	-10.20	-8.26	-11.70	-6.02	1.32	150
1.85	7.65	-1.68	-10.30	-8.24	-11.70	-6.03	1.37	151
1.9	7.68	-1.66	-10.40	-8.20	-11.60	-5.99	1.44	152
1.95	7.72	-1.62	-10.50	-8.16	-11.60	-5.95	1.51	153
2	7.74	-1.63	-10.60	-8.13	-11.50	-5.90	1.57	155
C.V.	1.8%	-2.3%	-4.9%	-3.1%	-2.4%	-1.4%	35.4%	4.9%

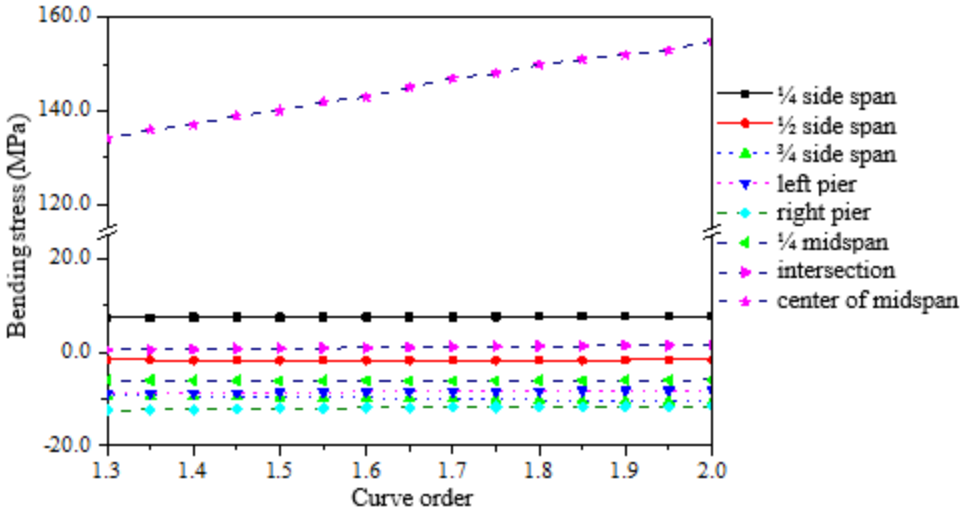

Figure 10. Stress at the Bottom Edge at Different Curve Orders.

4.1.3. Deformation

Table 9 and Figure 11 are the deformation of bridge at the important locations with the increase of curve order. The deformations demonstrate insignificant variation with coefficients of variation below 8%, indicating that the deformation is also not a key indicator of the bridge's performance with respect to curve orders.

Table 9. Deformations at Different Curve Orders (Unit: cm).

Curve order	¼ side span	½ side span	¾ side span	¼ midspan	Intersection	Center of midspan
1.3	-4.62	-5.53	-1.10	-27.00	-32.49	-46.88
1.35	-4.71	-5.64	-1.11	-27.37	-33.04	-47.64
1.4	-4.71	-5.69	-1.10	-27.61	-33.39	-48.14
1.45	-4.80	-5.81	-1.11	-28.00	-33.95	-48.90
1.5	-4.80	-5.84	-1.09	-28.25	-34.31	-49.40
1.55	-4.89	-5.98	-1.11	-28.67	-34.89	-50.15
1.6	-4.93	-6.24	-1.19	-28.41	-34.75	-50.51
1.65	-4.98	-6.16	-1.11	-29.36	-35.82	-51.37
1.7	-5.03	-6.26	-1.12	-29.69	-36.28	-51.97
1.75	-5.07	-6.35	-1.12	-30.06	-36.74	-52.54
1.8	-5.12	-6.48	-1.11	-30.55	-37.36	-53.32
1.85	-5.15	-6.55	-1.12	-30.77	-37.66	-53.69
1.9	-5.19	-6.65	-1.13	-31.12	-38.11	-54.24
1.95	-5.23	-6.75	-1.14	-31.47	-38.56	-54.79
2	-5.27	-6.84	-1.14	-31.82	-38.99	-55.33
C.V.	-7.3%	-2.3%	-5.7%	-6.3%	-5.7%	-4.5%

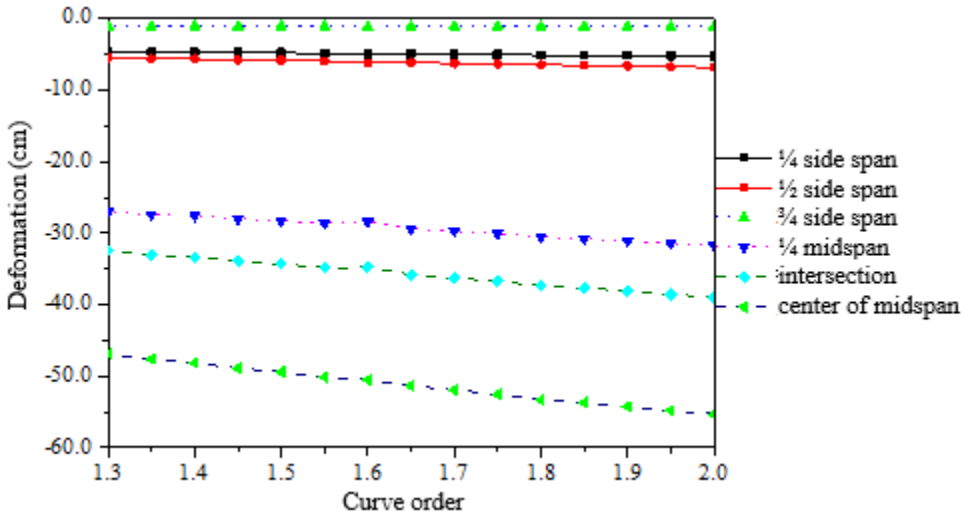

Figure 11. Deformation at Different Curve Orders.

4.1.4. Bending strain energy

The summation of bending strain energy of all the bridge elements are calculated at different curve orders. Though the bending strain energy shows an increasing trend with the increase of curve order, the maximum increase is only 10% at a curve order of 2.

Table 10. Bending Strain Energy at Different Curve Orders (Unit: kJ).

Curve order	1.3	1.35	1.4	1.45	1.5	1.55	1.6	1.65	1.7	1.75	1.8	1.85	1.9	1.95	2
Bending strain energy(kJ)	5526	5548	5574	5603	5630	5664	5616	5748	5790	5835	5893	5920	5974	6022	6069
Relative value	1.00	1.00	1.01	1.01	1.02	1.02	1.02	1.04	1.05	1.06	1.07	1.07	1.08	1.09	1.10

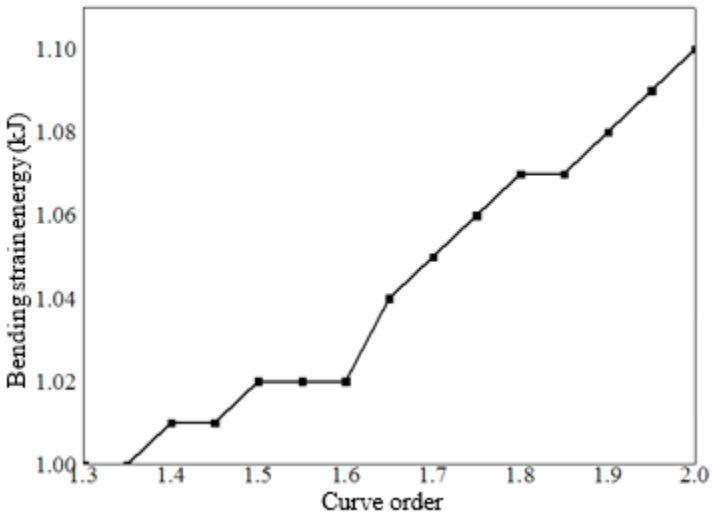

Figure 12. Bending Strain Energy at Different Curve Orders.

4.2. Optimization on Curve Order

It can be seen from the analysis above that when the curve order variates, the bending moments and stresses have the maximum of C.V. at the concrete-steel intersection. Therefore, taking the moments and stresses at the intersection as the objective function for, the optimal curve order happens at 1.3 where the stress reaches the minimum as well as the bending strain energy.

5. MIDSPAN DEPTH-TO-SPAN RATIO: PARAMETRIC ANALYSIS AND OPTIMIZATION

The depth-to-span ratio is not only the important part of the steel-concrete composite rigid frame bridges, but also one of the important parameters to design this type of bridge. This parameter can relate to the appearance of the bridge, the volume of work for the whole bridge, the arrangement of the prestressed, the clearance of the bridge and the mechanical performance. It also can directly affect the safety and durability of the bridges. The small depth-to-ratio has the advantages of light structure, low volume of work, low cost, etc. However, too small ratio may cause the stress and deformation of the structure not meeting the design requirements. In this chapter, depth-to-span rations are decided to two parts, namely midspan depth-to-span ratio which is without changing of the depth of box girder at the support and support depth-to-span ratio without changing of the depth of box girder at the midspan. From the experience of this type of the bridge, this chapter studied the range of the value and characteristics of midspan depth to span ratio, then built the numerical model, further analysis the relationship between midspan depth-to-span ratio, the weight of bridge and the force, finally provide the appropriate value of this ratio [38-40].

With the longer span of the prestressed concrete rigid frame bridges built, there are abundant experience to refer. However, the range value of the depth-to-ratio is not defined. The range of depth to span ratio of with the same high box-girders at the middle of box girder is 1/30 - 1/50. The range of support depth to span ratio of variational high box-girders is 1/16 - 1/25 [41]. When the main span is larger than 100m, the range support depth to span ratio of box girder to the main span is 1/17 - 1/21. When the main span is less than 100m, that ratio of box girder is 1/14 - 1/22. Generally, the depth of prestressed concrete straight box girders is the 1/18 - 1/20 of the main

span, support depth to span ratio of variational high box-girders is 1/16 - 1/20, and midspan depth to span ratio is 1/30 - 1/50. There are not definitely national codes about midspan and support depth to span ratio [42-44]. However, the data of the bridges built has the following characteristics: the depth to the span ratio of the same depth of the box girder is 1/13.3 - 1/28.3 and midspan depth to span ratio of variational high box-girders is l/34.6 - l/50, support midspan depth to span ratio of variational high box-girders is l/15.8 - l/20.2.

From the reference, generally the midspan depth-to-span ratio is 1/30 - 1/50 and the support depth-to-span ratio is 1/16 - 1/25 (Xue, Yuan, and Li 2012; Yang 2012). Compared to both ratios, the support depth to ratio is larger than the midspan depth-to-span ratio. Table 11 shows the depth of the girder at the support and midspan and the depth-to-span ratio.

Table 11. Examples of Depth-to-Span Ratio of Large-Span Rigid Frame Bridges.

Number	Bridge name	Length of midspan (L)	$H_{support}$	$H_{midspan}$	$H_{support}$ /L	$H_{midspan}$ /L
1	Humen	270	14.8	5	0.0548	0.0185
2	Huangshi Yangtze	245	13	4.1	0.0531	0.0167
3	Jinchangling Lancang	200	13	4	0.0650	0.0200
4	James River	205	12	4.9	0.0585	0.0239
5	Houston	228	14.6	4.6	0.0640	0.0202
6	Orwell	190	12	4	0.0632	0.0211
7	Donau	190	10.6	5	0.0558	0.0263
8	Tuas Second Link	165	10	3	0.0606	0.0182
9	Stolma	301	15	3.5	0.0498	0.0116
10	Gate Way	260	15	5.2	0.0577	0.0200

As shown in Table 11, the support depth-to-span ratio H /L distribution of prestressed concrete continuous rigid frame bridge is between 0.05 - 0.06, which is 1/20 - 1/16.7; and its average value is 1/17 in China, which is between 1/25 - 1/14.3, and its average value is 1/19 in other countries, which is between1/20 - 1/16.7. In China, the midspan depth-to-span ratio H/L is distributed between 1/40 and 1/73, and the value is mainly distributed between 1/55 and 1/66.7, of which average value is 1/58. In the other

countries, the midspan depth-to-span ratio H /L is distributed between 1/27.8 to 1/91, and the value is mainly distributed between 1/40 and 1/67, of which average value is 1/50.

5.1. Parametric Analysis on Depth-to-Span Ratio

Oujing bridge is used as the model, and software MIDAS CIVIL 2010 is used to build the different models with the different span depth-to-span ratio and support depth-to-span ratio to analysis the inert loads and the range of span depth to span ratio is between 1/30 to 1/72 with 22 different models and that of the support depth to span ratio is between 1/16 and 1/25 with different 10 models. Elements, joints, and the order of the construction of these 32 models are the same with the original ones, however the depth of the girders is different. The design of structure is focused on the bending moment, stress and displacement of the important section. The bending moment, stress and displacement of the structures are analyzed and compared with each other as follows.

5.1.1. Bending moments

Table 12 and Figure 13 lists and illustrates the bending moments and their trend of the important sections with different span depth to span ratio. The moments of middle of side span and the quarter of the middle span are increasing with the decreasing of the depth to span ratio, and conversely the other sections are decreasing. The moment at the middle of main span has the largest increase of 108679KN.m and that at the quarter of the main span has the largest decrease of 76445KN.m. The coefficient of variation reaches the maximum at the steel-concrete intersection, i.e., 110%, which indicates that the bridge girder’s span depth to ratio has the largest influence on the bending moment at the intersection.

Table 12. Bending Moments at Different Midspan Depth-to-Span Ratio (Unit: kN.m).

Depth-to-span ratio	¼ side span	½ side span	¾ side span	Left pier	Right pier	¼ midspan	Intersection	Center of midspan
1/30	108500	-2250	-358893	-911588	-1288320	-15844	84677	208334
1/32	104698	-5497	-358829	-911942	-1280542	-26817	70880	188008
1/34	101714	-7650	-356552	-904760	-1271986	-34245	62373	178692
1/36	99075	-9575	-354171	-897319	-1261915	-41074	54389	169555
1/38	96516	-11603	-353207	-893523	-1255881	-47119	47349	161675
1/40	94198	-13546	-352245	-889443	-1249739	-52636	41023	154405
1/42	91833	-15714	-351862	-885520	-1244226	-58466	34296	146927
1/44	89913	-17290	-350983	-882694	-1236896	-61103	30970	143091
1/46	85900	-21493	-353125	-882452	-1231656	-65176	26185	137534
1/48	86088	-20941	-350782	-878321	-1226499	-68405	22350	133187
1/50	84314	-22720	-350951	-876714	-1221947	-71341	18898	129286
1/52	82614	-24482	-351288	-875448	-1217370	-74040	15645	125598
1/54	80993	-26205	-351736	-874591	-1213129	-76979	12108	121237
1/56	79439	-27943	-352395	-874068	-1209505	-79230	9467	118223
1/58	77904	-29638	-353055	-873531	-1205338	-81309	6860	115247
1/60	76423	-31349	-353852	-873283	-1201769	-83188	4586	112648
1/62	74959	-33118	-354946	-873651	-1198898	-85054	2370	110144
1/64	73637	-34669	-355752	-873491	-1195518	-86656	382	107754
1/66	72324	-36287	-356776	-874088	-1193605	-88561	-1692	105406
1/68	71008	-37918	-357867	-874429	-1189789	-89850	-3492	103269
1/70	71101	-37712	-356899	-874460	-1197001	-93173	-5324	105347
1/72	68519	-41096	-360181	-875700	-1183745	-92289	-6649	99655
C.V.	14%	-50%	-1%	-1%	-3%	-33%	110%	23%

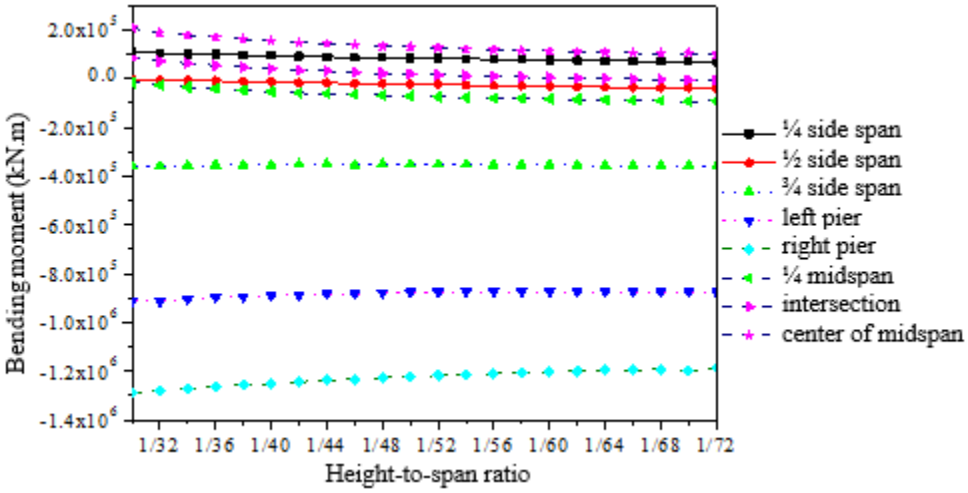

Figure 13. Bending Moment at Different Depth-to-Span Ratios.

5.1.2. Stresses

Table 13 tabulates the Stresses at the top edge of the important cross sections at different span depth to span ratio, which is also shown in Figure 14. The stresses at middle of main span, the left pier, the right pier, and the steel-concrete intersection are decreasing with the decreasing of the depth to span ratio, and conversely the other sections are increasing. The stress at the top edge at the middle of main span has the largest increase of 23.5MPa and that at steel-concrete intersection has the largest decrease of 1.65MPa. The coefficient of variation reaches the maximum at the steel-concrete intersection, i.e., 75%, which indicates that the span depth to span ratio has the largest influence on the stress at the intersection.

Table 14 tabulates the Stresses at the bottom edge of the important cross sections at different span depth to span ratio, which is also shown in Figure 15. The stresses at middle of main span, the left pier, the right pier, and the steel-concrete intersection are decreasing with the decreasing of the depth to span ratio, and conversely the other sections are increasing. The stress at the bottom edge at the middle of main span has the largest increase of 35MPa and that at steel-concrete intersection has the largest decrease of 2.6MPa. The coefficient of variation reaches the maximum at the steel-concrete intersection, i.e., 123%, which indicates that the span depth to span ratio has the largest influence on the stress at the intersection.

Table 13. Stresses at the Top Edge at Different Midspan Depth-to-Span Ratios (Unit: MPa).

Depth-to-span ratio	¼ side span	½ side span	¾ side span	Left pier	Right pier	¼ midspan	Intersection	Center of midspan
1/30	-2.74	0.03	6.46	7.26	10.2	0.23	-1.39	-77.5
1/32	-2.87	0.11	6.39	7.27	10.2	0.53	-1.29	-75.6
1/34	-3.02	0.17	6.53	7.21	10.1	0.78	-1.25	-77
1/36	-3.17	0.23	6.67	7.15	10	1.04	-1.2	-78.1
1/38	-3.31	0.30	6.8	7.12	9.98	1.30	-1.14	-79.2
1/40	-3.45	0.38	6.93	7.08	9.92	1.57	-1.08	-80.3
1/42	-3.59	0.47	7.06	7.05	9.88	1.88	-0.99	-80.6
1/44	-3.74	0.54	7.17	7.03	9.82	2.08	-0.97	-82.8
1/46	-4.02	0.71	7.34	7.02	9.78	2.36	-0.90	-83.8
1/48	-4.03	0.72	7.4	6.99	9.74	2.62	-0.83	-85.2
1/50	-4.18	0.81	7.53	6.98	9.7	2.88	-0.77	-86.5
1/52	-4.32	0.91	7.64	6.97	9.66	3.14	-0.70	-87.8
1/54	-4.46	1.01	7.75	6.96	9.63	3.43	-0.60	-88.7
1/56	-4.61	1.12	7.86	6.96	9.6	3.7	-0.53	-90.1
1/58	-4.75	1.23	7.96	6.95	9.56	3.98	-0.44	-91.4
1/60	-4.89	1.35	8.07	6.95	9.53	4.25	-0.36	-92.8
1/62	-5.03	1.47	8.17	6.95	9.51	4.53	-0.27	-94.1
1/64	-5.18	1.58	8.28	6.95	9.48	4.8	-0.17	-95.9
1/66	-5.31	1.7	8.38	6.95	9.47	5.1	-0.06	-96.9
1/68	-5.46	1.83	8.47	6.96	9.43	5.37	0.04	-98.2
1/70	-5.46	1.85	8.51	6.94	9.47	5.74	0.13	-97.2
1/72	-5.74	2.09	8.67	6.97	9.38	5.93	0.26	-101
C.V.	-22%	67%	10%	2%	3%	58%	-75%	-9%

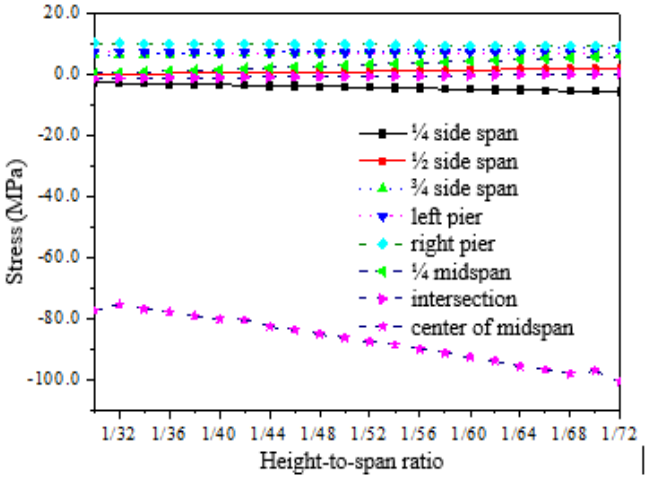

Figure 14. Stress at the Top Edge at Different Midspan Depth-to-Span Ratio.

Table 14. Stresses at the Bottom Edge at Different Midspan Depth-to-Span Ratios (Unit: MPa).

Depth-to-span ratio	¼ side span	½ side span	¾ side span	Left pier	Right pier	¼ midspan	Intersection	Center of midspan
1/30	4.49	-0.09	-8.22	-8.8	-12.5	-0.76	1.86	119
1/32	4.71	-0.22	-7.96	-8.8	-12.4	-1.28	1.69	117
1/34	4.95	-0.31	-8.13	-8.74	-12.3	-1.7	1.6	118
1/36	5.2	-0.40	-8.32	-8.66	-12.2	-2.13	1.5	120
1/38	5.44	-0.51	-8.44	-8.63	-12.2	-2.57	1.4	121
1/40	5.68	-0.62	-8.59	-8.59	-12.1	-3.02	1.29	124
1/42	5.91	-0.75	-8.75	-8.55	-12	-3.51	1.15	124
1/44	6.15	-0.86	-8.88	-8.53	-12	-3.87	1.1	127
1/46	6.6	-1.1	-9.08	-8.52	-11.9	-4.32	0.98	129
1/48	6.62	-1.11	-9.15	-8.49	-11.9	-4.74	0.87	130
1/50	6.85	-1.25	-9.3	-8.47	-11.8	-5.17	0.77	132
1/52	7.07	-1.4	-9.43	-8.46	-11.8	-5.59	0.66	134
1/54	7.3	-1.55	-9.55	-8.45	-11.8	-6.05	0.51	137
1/56	7.51	-1.7	-9.68	-8.45	-11.7	-6.49	0.40	139
1/58	7.74	-1.86	-9.8	-8.44	-11.7	-6.92	0.27	140
1/60	7.95	-2.03	-9.92	-8.44	-11.6	-7.35	0.14	142
1/62	8.16	-2.2	-10	-8.44	-11.6	-7.79	0.01	144
1/64	8.38	-2.36	-10.2	-8.44	-11.6	-8.21	-0.13	145
1/66	8.58	-2.53	-10.3	-8.45	-11.6	-8.68	-0.28	149
1/68	8.8	-2.72	-10.4	-8.45	-11.5	-9.1	-0.43	151
1/70	8.78	-2.77	-10.5	-8.46	-11.6	-9.77	-0.62	160
1/72	9.2	-3.08	-10.6	-8.47	-11.5	-9.95	-0.74	154
C.V.	21%	-64%	-9%	-1%	-3%	-53%	123%	9%

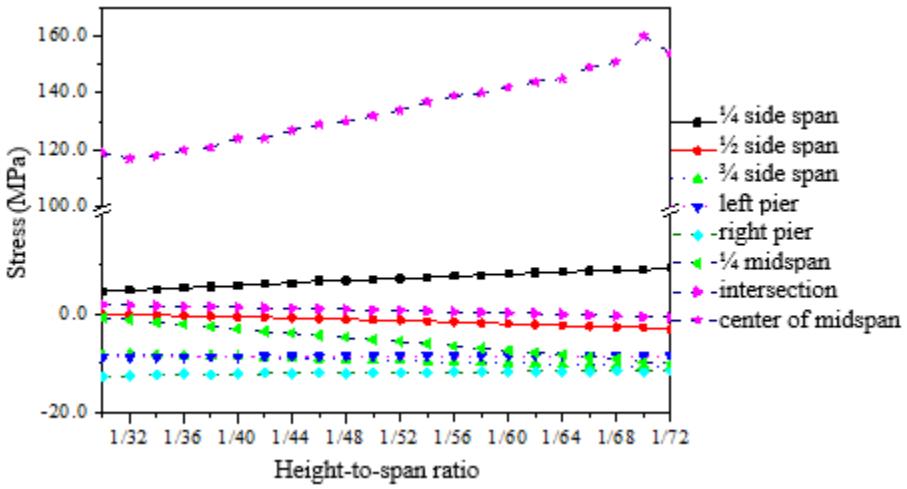

Figure 15. Stress at the Bottom Edge at Different Depth-to-Span Ratios.

5.1.3. Deformations

Table 15 and Figure 16 are the deformation of bridge at the important locations with the decrease of span depth to span ratio. With the increase of the span depth to span ratio, the deformations are increasing. The deformation at the middle of main span has the largest increase of 20.43cm. The coefficient of variation reaches the maximum at middle of the side span, i.e., 64%, which indicates that the span depth to span ratio has the largest influence on the deformation at middle of side span.

Table 15. Deformations at Different Midspan Depth-to-Span Ratios (Unit: cm).

Depth-to-span ratio	¼ side span	½ side span	¾ side span	Left pier	Right pier	Center of midspan
1/30	-1.62	-3.68	-0.76	-22.74	-25.09	-30.66
1/32	-1.83	-3.76	-0.81	-22.54	-25.07	-31.14
1/34	-2.05	-3.94	-0.82	-23.09	-25.91	-32.72
1/36	-2.27	-4.16	-0.85	-23.65	-26.77	-34.36
1/38	-2.51	-4.34	-0.88	-24.11	-27.51	-35.83
1/40	-2.75	-4.54	-0.90	-24.63	-28.34	-37.44
1/42	-2.99	-4.72	-0.92	-25.17	-29.21	-38.47
1/44	-3.26	-4.94	-0.97	-25.53	-29.83	-40.53
1/46	-3.77	-5.21	-1.02	-25.95	-30.53	-42.10
1/48	-3.80	-5.34	-1.03	-26.41	-31.32	-43.71
1/50	-4.09	-5.54	-1.07	-26.84	-32.06	-45.30
1/52	-4.38	-5.74	-1.10	-27.24	-32.77	-46.86
1/54	-4.67	-5.94	-1.14	-27.65	-33.50	-48.54
1/56	-4.98	-6.14	-1.17	-28.07	-34.25	-50.21
1/58	-5.29	-6.34	-1.21	-28.43	-34.93	-51.79
1/60	-5.60	-6.54	-1.24	-28.81	-35.64	-53.44
1/62	-5.92	-6.72	-1.27	-29.14	-36.28	-55.04
1/64	-6.25	-6.93	-1.31	-29.54	-37.01	-56.76
1/66	-6.57	-7.12	-1.34	-29.94	-37.77	-58.63
1/68	-6.92	-7.32	-1.38	-30.24	-38.39	-60.23
1/70	-6.89	-7.34	-1.35	-31.06	-39.80	-63.28
1/72	-7.62	-7.71	-1.46	-30.87	-39.68	-63.67
C.V.	21%	-64%	-9%	-1%	-3%	-53%

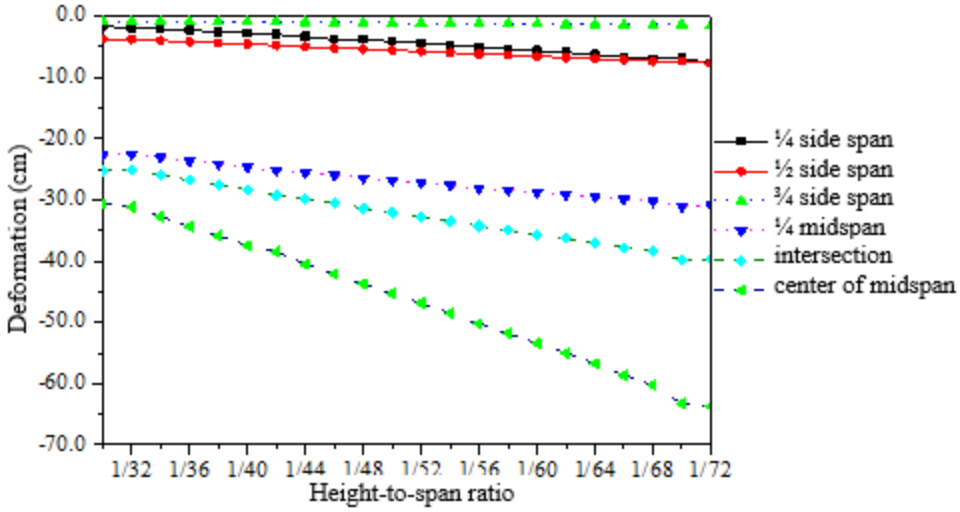

Figure 16. Deformation at Different Depth-to-Span Ratios.

5.1.4. Bending strain energy

Table 16 and Figure 17 illustrate the variation of bending strain energy with the midspan depth-to-span ratio. A ratio of 1/32 has the minimum value of bending strain energy, while a ratio of 1/70 leads to the maximum of bending strain energy.

Table 16. Bending Strain Energy at Different Midspan Depth-to-Span Ratios (Unit: kJ).

Depth-to-Span Ratio	1/30	1/32	1/34	1/36	1/38	1/40	1/42	1/44	1/46	1/48	1/50
Bending strain energy (kJ)	4571	4463	4538	4608	4679	4759	4825	4908	5004	5066	5148
Relative value	1.11	1.08	1.10	1.12	1.14	1.15	1.00	1.19	1.21	1.23	1.07
Depth-to-Span Ratio	1/52	1/54	1/56	1/58	1/60	1/62	1/64	1/66	1/68	1/70	1/72
Bending strain energy (kJ)	5227	5306	5392	5470	5554	5631	5769	5819	5894	6101	6062
Relative value	1.27	1.29	1.31	1.33	1.35	1.37	1.40	1.41	1.43	1.48	1.47

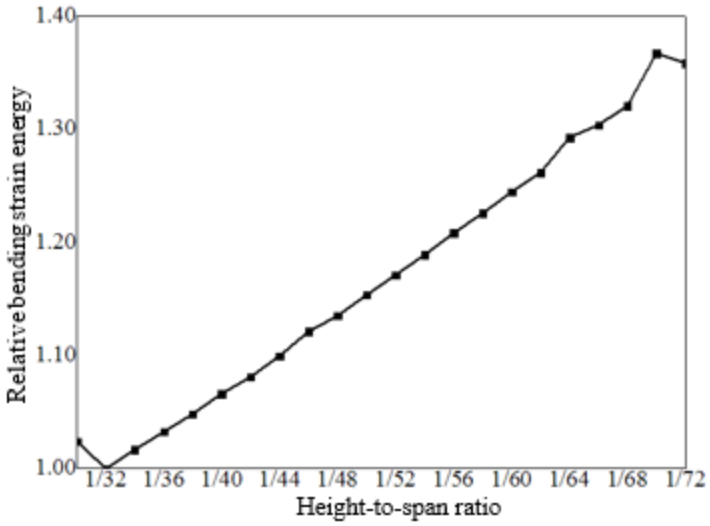

Figure 17. Relative Bending Strain Energy at Different Depth-to-Span Ratios.

5.2. Optimization on Midspan Depth-to-Span Ratio

It can be seen from the analysis above that when the midspan depth-to-span ratio variates, the bending moments and stresses have the maximum of C.V. at the concrete-steel intersection. Therefore, the structural optimization takes the moments and stresses at the intersection as the objective function. The bending moment at the intersection reaches the minimum, i.e., 382 kN.m at the ratio of 1/64; the top stress reaches the minimum, 0.04 MPa at 1/68; the bottom stress reaches the minimum, 0.01 MPa, at 1/62. On the other hand, a ratio of 1/32 has the minimum value of bending strain energy. With the preference of uniform distribution of bending moment, the midspan depth-to-span ratio is optimized at 1/32.

6. SUPPORT DEPTH-TO-SPAN RATIO: PARAMETRIC ANALYSIS AND OPTIMIZATION

6.1. Parametric Analysis on Depth-to-Span Ratio

6.1.1. Bending moments

Table 17 and Figure 18 demonstrate the bending moments at significant intersections with the variation of the support depth-to-span ratio. It can be seen that with the decrease of the ratio, the bending moments increase at the ¼ side span, the midspan and the steel-concrete intersection that changes from negative moment to positive moment and decrease at other cross sections. The midspan bending moment has the maximum increase, i.e., 34490 kN.m, while the bending moment decreases the most at the left-pier cross section that is 140723 kN.m. The C.V. has the minimum value at the right-pier cross section and the maximum at the steel-concrete intersection, which are -2% and 87%, respectively.

Table 17. Bending Moments at Different Depth-to-Span Ratios (Unit: kN.m).

Depth-to-span ratio	¼ side span	½ side span	¾ side span	Left pier	Right pier	¼ midspan	Intersection	Center of midspan
1/16	63889	-58087	-406580	-981023	-1288674	-97806	-4234	115649
1/17	66648	-52717	-396622	-961116	-1276459	-93786	-219	119653
1/18	69295	-47569	-387208	-942610	-1265443	-89840	3759	123621
1/19	71840	-42628	-378283	-925306	-1255265	-85936	7698	127550
1/20	74286	-37881	-369800	-909052	-1245771	-82068	11597	131440
1/21	76638	-33322	-361731	-893742	-1236855	-78231	15463	135298
1/22	78856	-29025	-354166	-879614	-1228484	-74457	19264	139092
1/23	81103	-24741	-346772	-865637	-1220483	-70652	23094	142914
1/24	83186	-20645	-339640	-852390	-1212900	-66904	26866	146678
1/25	85110	-16922	-333194	-840300	-1205950	-63460	30331	150139
C.V.	10%	-38%	-7%	-5%	-2%	-14%	87%	9%

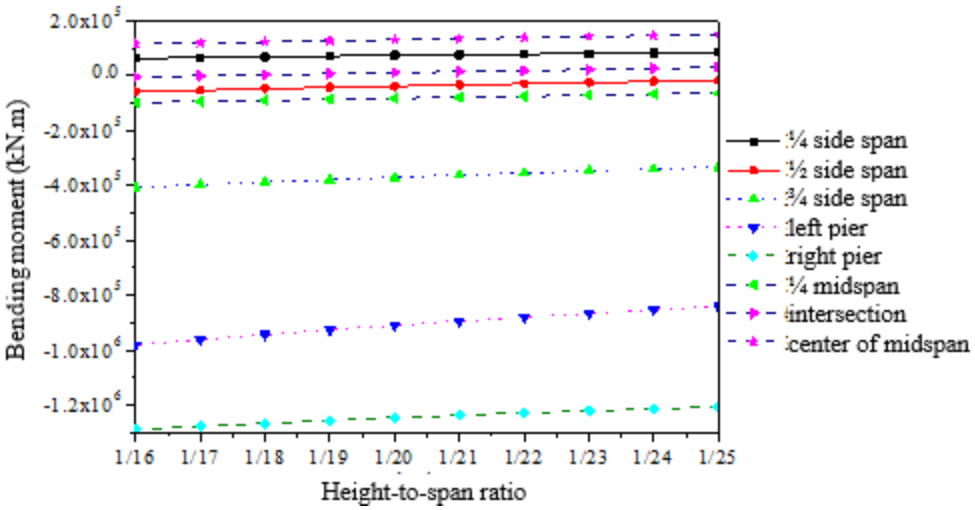

Figure 18. Bending Moment at Different Depth-to-Span Ratios.

6.1.2. Stresses

Table 18 tabulates the Stresses at the top edge of the important cross sections at different support depth-to-span ratio, which is also shown in Figure 19. The top-edge stresses at ½ side span, ¼ midspan, and the steel-concrete intersection are decreasing with the decrease of the depth to span ratio, and conversely the stressed at other sections are increasing. The stress at the top edge at the middle of main span has the largest increase of 18.7MPa and that at ¼ midspan has the largest decrease of 1.29MPa. The coefficient of variation reaches the maximum at the steel-concrete intersection, i.e., 75%, which indicates that the span depth to span ratio has the largest influence on the stress at the intersection.

Table 19 tabulates the stresses at the bottom edge of the important cross sections at different support depth to span ratio, which is also shown in Figure 20. The stresses at ½ side span, ¼ midspan, and the steel-concrete intersection are decreasing with the decrease of the depth to span ratio, and conversely the other sections are increasing. The stress at the bottom edge at midspan has the largest increase of 36 MPa and that at ¼ midspan intersection has the largest decrease of 1.99 MPa. The coefficient of variation reaches the maximum at the steel-concrete intersection, i.e.,

109%, which indicates that the support depth to span ratio has the largest influence on the stress at the intersection.

Table 18. Stresses at the Top Edge at Different Depth-to-Span Ratios (Unit: MPa).

Depth-to-span ratio	¼ side span	½ side span	¾ side span	Left pier	Right pier	¼ midspan	Intersection	Center of midspan
1/16	-3.71	1.97	6.37	4.59	6.01	4.24	0.02	-65.3
1/17	-3.87	1.85	6.65	4.98	6.59	4.12	-0.14	-67.5
1/18	-4.02	1.72	6.92	5.38	7.19	3.99	-0.31	-69.7
1/19	-4.17	1.59	7.17	5.79	7.83	3.86	-0.47	-71.8
1/20	-4.31	1.45	7.41	6.21	8.48	3.72	-0.63	-73.9
1/21	-4.45	1.3	7.64	6.64	9.16	3.57	-0.79	-76
1/22	-4.58	1.16	7.86	7.08	9.86	3.42	-0.95	-78
1/23	-4.71	1	8.06	7.53	10.6	3.26	-1.1	-80.1
1/24	-4.83	0.851	8.25	7.98	11.3	3.1	-1.26	-82.1
1/25	-4.94	0.707	8.44	8.44	12.1	2.95	-1.4	-84
C.V.	-10%	32%	9%	20%	23%	12%	-68%	-8%

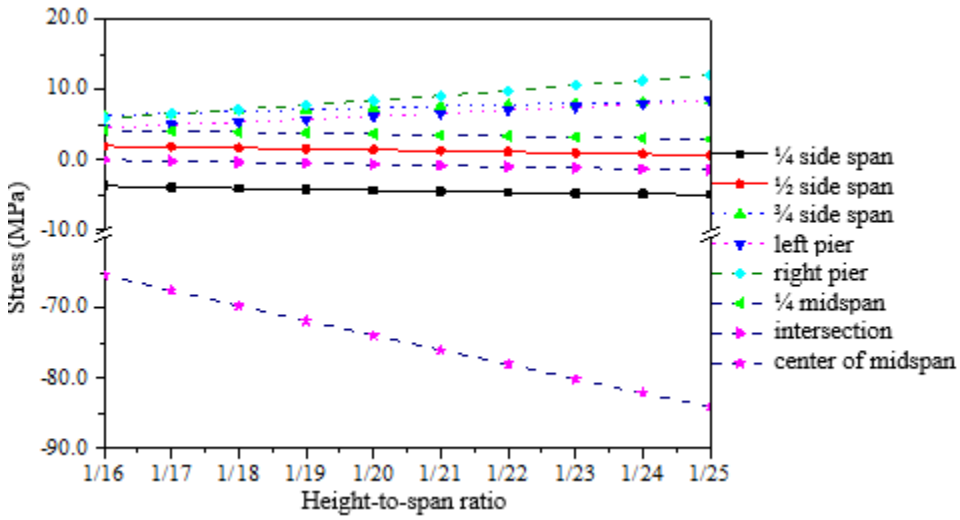

Figure 19. Stress at the Top Edge at Different Depth-to-Span Ratios.

Table 19. Stresses at the Bottom Edge at Different Depth-to-Span Ratios (Unit: MPa).

Depth-to-span ratio	¼ side span	½ side span	¾ side span	Left pier	Right pier	¼ midspan	Intersection	Center of midspan
1/16	6.05	-2.98	-8.11	-6.33	-8.33	-7.39	-0.39	118
1/17	6.31	-2.8	-8.4	-6.74	-8.98	-7.21	-0.16	122
1/18	6.56	-2.6	-8.68	-7.17	-9.65	-7.02	0.06	127
1/19	6.81	-2.4	-8.95	-7.62	-10.4	-6.81	0.28	131
1/20	7.04	-2.18	-9.21	-8.07	-11.1	-6.59	0.50	135
1/21	7.26	-1.97	-9.45	-8.53	-11.8	-6.36	0.72	139
1/22	7.47	-1.75	-9.68	-9	-12.6	-6.13	0.93	143
1/23	7.68	-1.53	-9.9	-9.46	-13.4	-5.88	1.15	147
1/24	7.88	-1.3	-10.1	-9.93	-14.2	-5.63	1.36	151
1/25	8.06	-1.09	-10.3	-10.4	-15	-5.4	1.55	154
C.V.	10%	-31%	-8%	-17%	-19%	-11%	109%	9%

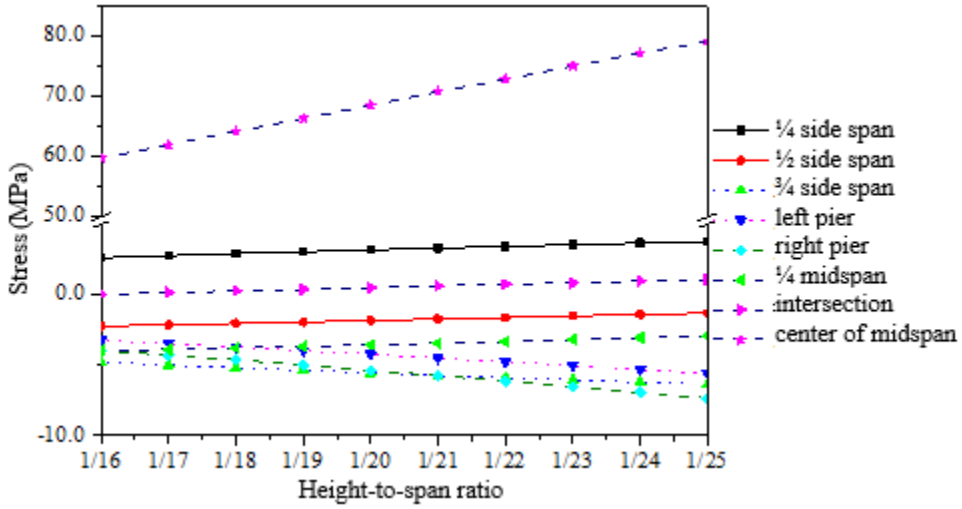

Figure 20. Stress at the Bottom Edge at Different Depth-to-Span Ratios.

6.1.3. Deformations

Table 20 and Figure 21 are the deformation of bridge at the important locations with the decrease of support depth to span ratio. With the decrease of the span depth to span ratio, the deformation is increasing. The deformation at the midspan has the largest increase of 19.74 cm. The coefficient of variation reaches the maximum at ¾ side span, i.e., 62%, which indicates that the support depth to span ratio has the largest influence on the deformation at ¾ side span.

Table 20. Deformations at Different Depth-to-Span Ratios (Unit: cm).

Depth-to-span ratio	¼ side span	½ side span	¾ side span	Left pier	Right pier	Center of midspan
1/16	-3.54	-2.81	-0.14	-18.50	-23.43	-37.13
1/17	-3.77	-3.30	-0.28	-20.07	-25.24	-39.29
1/18	-3.99	-3.80	-0.42	-21.68	-27.09	-41.46
1/19	-4.22	-4.33	-0.58	-23.34	-28.96	-43.65
1/20	-4.45	-4.87	-0.75	-25.04	-30.87	-45.85
1/21	-4.67	-5.44	-0.93	-26.77	-32.80	-48.05
1/22	-4.89	-6.01	-1.12	-28.51	-34.73	-50.25
1/23	-5.13	-6.64	-1.33	-30.34	-36.74	-52.50
1/24	-5.35	-7.25	-1.55	-32.18	-38.75	-54.74
1/25	-5.53	-7.85	-1.77	-33.98	-40.69	-56.87
C.V.	-15%	-33%	-62%	-20%	-18%	-14%

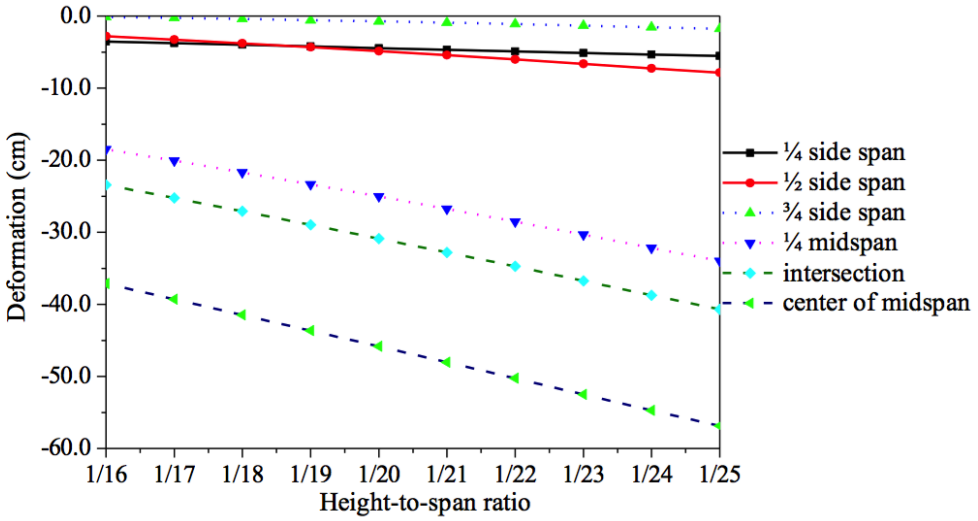

Figure 21. Deformation at Different Support Depth-to-Span Ratios.

6.1.4. Bending strain energy

Table 21 and Figure 22 illustrate the variation of bending strain energy with the support depth-to-span ratio. A ratio of 1/16 has the minimum value of bending strain energy, while a ratio of 1/25 leads to the maximum of bending strain energy.

Table 21. Bending Strain Energy at Different Depth-to-Span Ratios (Unit: kJ).

Depth-to-span ratio	1/16	1/17	1/18	1/19	1/20	1/21	1/22	1/23	1/24	1/25
Bending strain energy	3628	3941	4264	4595	4934	5281	5628	5999	6367	6742
Relative value	1.00	1.09	1.18	1.27	1.36	1.46	1.55	1.65	1.76	1.86

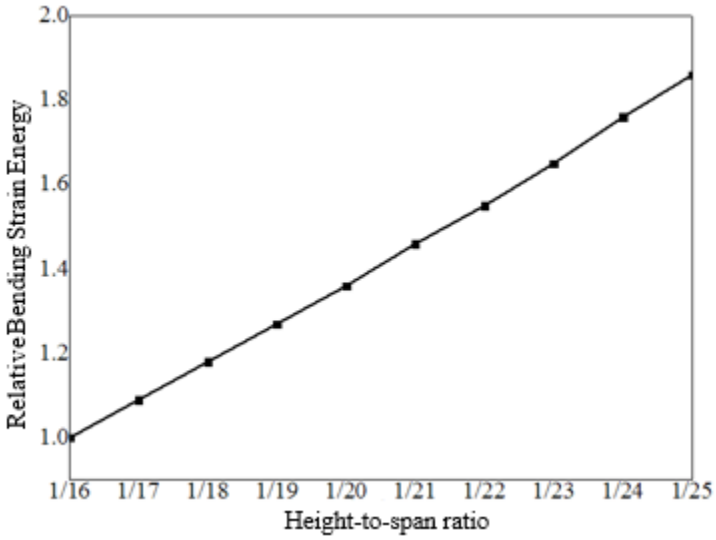

Figure 22. Bending Strain Energy at Different Support Depth-to-Span Ratios.

6.2. Optimization on Support Depth-to-Span Ratio

It can be seen from the analysis above that when the support depth-to-span ratio variates, the bending moments and stresses have the maximum of C.V. at the concrete-steel intersection. Therefore, the structural optimization takes the moments and stresses at the intersection as the objective function. The bending moment at the intersection reaches the minimum, i.e., -219 kN.m at the ratio of 1/17; the top stress reaches the minimum, 0.02 MPa at 1/16; the bottom stress reaches the minimum, 0.06 MPa, at 1/18. On the other hand, a ratio of 1/16has the minimum value of bending strain energy. With the preference of uniform distribution of bending moment, the midspan depth-to-span ratio is optimized at 1/16.

7. COMPUTER PROGRAM DEVELOPMENT FOR MATRIX STIFFNESS STRUCTURAL ANALYSIS

This chapter develops the computer program for bridge structural analysis using matrix stiffness method. The program can be used for further analysis in the future, e.g. advanced structural optimization, nonlinear analysis, etc. It is suitable for the matrix stiffness method to analyze complex structures using computer. This method is the most common conduction of the FEM. First, the system must be modeled as a set of simpler, idealized elements interconnected at the nodes in applying the method. Second, the material stiffness properties of these elements are compiled into a single matrix equation through matrix mathematics. Third, the solution of this equation can determine the structure's unknown displacements and forces. The direct stiffness method forms the basis for most commercial and free source finite element software [46].

7.1. Implementation of Matrix Stiffness Method

This part is about the theoretical implementation of matrix stiffness method based on frame structures and frame elements. This work begins with the structural discretization, followed by the degree of freedom of frame element, element stiffness matrix, coordinate systems, global stiffness matrix, load assembly, and problem solving and internal force and reaction calculation. It lays the foundation for the program development in **7.2.**

7.1.1. Structural discretization

Determining the individual elements is the first step of the stiffness method. The structure is discretized and divided into more than one elements where there is a bearing support, a variation in material property, cross section area or moment of inertia, or where more than one components positioned in different directions intersect. While determining the elements, the structure is discretized at the nodes which are used to connect the different elements together. Member

stiffness equations are formed through analysis of each element. The forces and displacements are related to the element stiffness matrix which depends on the geometry and properties of the element.

7.1.2. Degree of freedom

The frame element in this study for rigid frame bridge analysis has three degree of freedoms (DOF) at each node with two for translation and one for rotation, and the truss element has two DOFs of translation, as is shown in Figure 23.

Figure 23. Degree of Freedom of Frame Element.

7.1.3. Element stiffness matrix

The local element stiffness matrix of frame element is expressed in Equation 6 based on its DOF as shown in Figure 23,

$$[k_L]=\begin{bmatrix} \frac{EA}{L} & 0 & 0 & -\frac{EA}{L} & 0 & 0 \\ 0 & \frac{12EI}{L^3} & \frac{6EI}{L^2} & 0 & -\frac{12EI}{L^3} & \frac{6EI}{L^2} \\ 0 & \frac{6EI}{L^2} & \frac{4EI}{L} & 0 & -\frac{6EI}{L^2} & \frac{2EI}{L} \\ -\frac{EA}{L} & 0 & 0 & \frac{EA}{L} & 0 & 0 \\ 0 & -\frac{12EI}{L^3} & -\frac{6EI}{L^2} & 0 & \frac{12EI}{L^3} & -\frac{6EI}{L^2} \\ 0 & \frac{6EI}{L^2} & \frac{2EI}{L} & 0 & -\frac{6EI}{L^2} & \frac{4EI}{L} \end{bmatrix} \quad (5)$$

where k_L is the local element stiffness, E is the modulus of elasticity, A is the area of element cross section, L is the element length, and I is the moment of inertia.

7.1.4. Coordinate systems

There are two coordinate systems for the structural analysis, i.e. the global coordinate system and the local element coordinate system, as indicated in Figure 24 by XOY and xoy, respectively.

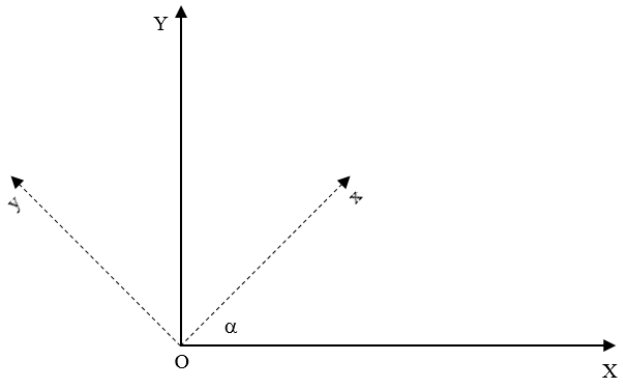

Figure 24. Coordinate Systems for Structural Analysis.

After we get the stiffness matrices of all the frame elements of a structure, we need to transform the stiffness matrices to the global coordinate system before we assemble them to form the global stiffness matrix. The same transformation needs to be done for displacement and force vectors. The matrix for coordinate transformation is as shown in Equation 7.

$$[T]=\begin{bmatrix} \cos\alpha & \sin\alpha & 0 & 0 & 0 & 0 \\ -\sin\alpha & \cos\alpha & 0 & 0 & 0 & 0 \\ 0 & 0 & 1 & 0 & 0 & 0 \\ 0 & 0 & 0 & \cos\alpha & \sin\alpha & 0 \\ 0 & 0 & 0 & -\sin\alpha & \cos\alpha & 0 \\ 0 & 0 & 0 & 0 & 0 & 1 \end{bmatrix} \tag{6}$$

7.1.5. Global stiffness matrix

Once the individual element stiffness matrices have been developed, they must be assembled into the original structure. The first step in this process is to convert the stiffness

relations for the individual elements into a global system by the coordinate transformation matrix as shown in Equation 7.

After forming the element stiffness matrix in the global coordinate system, the elements must be merged into a single global stiffness matrix. The merging process follows the principle of compatibility of displacements and force equilibrium at each node. These rules are confirmed and supported by relating the element nodal displacements to the global nodal displacements.

The global displacement and force vectors each contain one entry for each degree of freedom in the structure. The element stiffness matrices are merged by augmenting or expanding each matrix in conformation to the global displacement and load vectors.

Finally, the global stiffness matrix is developed by adding the individual expanded element matrices together.

Figure 25 (a) shows an example frame structure consisting of two members. The material properties and geometric dimensions are uniform along the structure for simplicity. It has a uniform loading on the beam, a concentrated force at the intersection of beam and column, and a concentrated force at the midpoint of the column. The frame is discretized into two frame elements following the discretization rule described in **7.1.1** ending up with three nodes and 9 degree of freedoms in total, as is illustrated in Figure 25 (b). Then the stiffness matrices of Elements 1 and 2, by Equation 6, are as shown in Equation 8.

$$[k_{\mathrm{L}}^{1}]=[k_{\mathrm{L}}^{2}]=\begin{bmatrix} \frac{EA}{L} & 0 & 0 & -\frac{EA}{L} & 0 & 0 \\ 0 & \frac{12EI}{L^3} & \frac{6EI}{L^2} & 0 & -\frac{12EI}{L^3} & \frac{6EI}{L^2} \\ 0 & \frac{6EI}{L^2} & \frac{4EI}{L} & 0 & -\frac{6EI}{L^2} & \frac{2EI}{L} \\ -\frac{EA}{L} & 0 & 0 & \frac{EA}{L} & 0 & 0 \\ 0 & -\frac{12EI}{L^3} & -\frac{6EI}{L^2} & 0 & \frac{12EI}{L^3} & -\frac{6EI}{L^2} \\ 0 & \frac{6EI}{L^2} & \frac{2EI}{L} & 0 & -\frac{6EI}{L^2} & \frac{4EI}{L} \end{bmatrix} \tag{7}$$

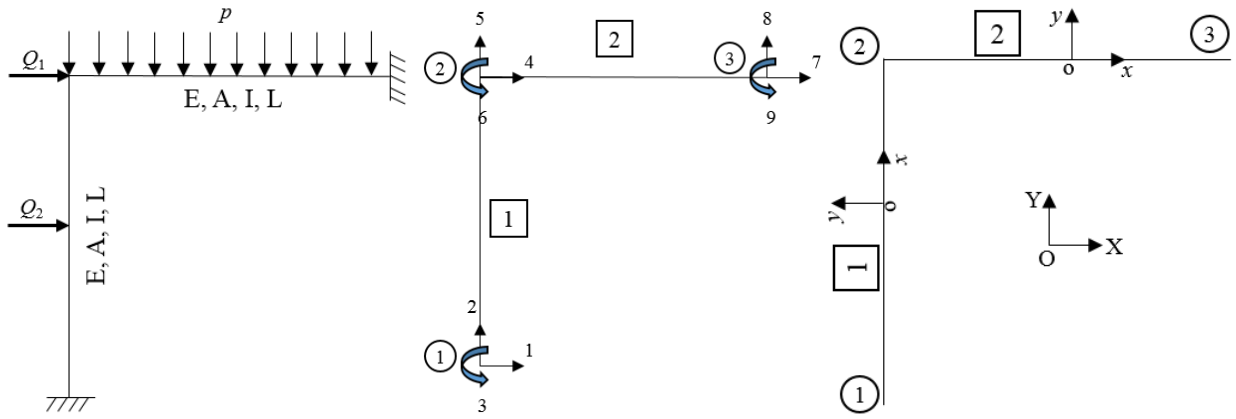

(a) frame structure (b) discretization (c) coordinate system

Figure 25. Example Frame Structure and its Discretization and Coordinate System.

The local coordinate system of Element 1 has angle of 90° with respect to the global coordinate system, then its transformation matrix is calculated in Equation 9 by Equation 7. Then the global stiffness matrix is as shown in Equation 10.

$$[T_1]=\begin{bmatrix} \cos 90^{o} & \sin 90^{o} & 0 & 0 & 0 & 0 \\ -\sin 90^{o} & \cos 90^{o} & 0 & 0 & 0 & 0 \\ 0 & 0 & 1 & 0 & 0 & 0 \\ 0 & 0 & 0 & \cos 90^{o} & \sin 90^{o} & 0 \\ 0 & 0 & 0 & -\sin 90^{o} & \cos 90^{o} & 0 \\ 0 & 0 & 0 & 0 & 0 & 1 \end{bmatrix}=\begin{bmatrix} 0 & 1 & 0 & 0 & 0 & 0 \\ -1 & 0 & 0 & 0 & 0 & 0 \\ 0 & 0 & 1 & 0 & 0 & 0 \\ 0 & 0 & 0 & 0 & 1 & 0 \\ 0 & 0 & 0 & -1 & 0 & 0 \\ 0 & 0 & 0 & 0 & 0 & 1 \end{bmatrix} \tag{8}$$

$$[k_{\mathrm{G}}^{1}]=[T_1]^T[k_{\mathrm{L}}^{1}][T_1]=\begin{bmatrix} \frac{12EI}{L^3} & 0 & -\frac{6EI}{L^2} & -\frac{12EI}{L^3} & 0 & -\frac{6EI}{L^2} \\ 0 & \frac{EA}{L} & 0 & 0 & -\frac{EA}{L} & 0 \\ -\frac{6EI}{L^2} & 0 & \frac{4EI}{L} & \frac{6EI}{L^2} & 0 & \frac{2EI}{L} \\ -\frac{12EI}{L^3} & 0 & \frac{6EI}{L^2} & \frac{12EI}{L^3} & 0 & \frac{6EI}{L^2} \\ 0 & -\frac{EA}{L} & 0 & 0 & \frac{EA}{L} & 0 \\ -\frac{6EI}{L^2} & 0 & \frac{2EI}{L} & \frac{6EI}{L^2} & 0 & \frac{4EI}{L} \end{bmatrix} \tag{9}$$

The local coordinate system of Element 2 is positioned the same along the global coordinate system, so its global stiffness matrix is the same with its local stiffness matrix, as is shown in Equation 9.

$$[k_{\mathrm{G}}^{2}]=[k_{\mathrm{L}}^{2}]=\begin{bmatrix} \frac{EA}{L} & 0 & 0 & -\frac{EA}{L} & 0 & 0 \\ 0 & \frac{12EI}{L^3} & \frac{6EI}{L^2} & 0 & -\frac{12EI}{L^3} & \frac{6EI}{L^2} \\ 0 & \frac{6EI}{L^2} & \frac{4EI}{L} & 0 & -\frac{6EI}{L^2} & \frac{2EI}{L} \\ -\frac{EA}{L} & 0 & 0 & \frac{EA}{L} & 0 & 0 \\ 0 & -\frac{12EI}{L^3} & -\frac{6EI}{L^2} & 0 & \frac{12EI}{L^3} & -\frac{6EI}{L^2} \\ 0 & \frac{6EI}{L^2} & \frac{2EI}{L} & 0 & -\frac{6EI}{L^2} & \frac{4EI}{L} \end{bmatrix} \tag{10}$$

The assembly of the global stiffness matrix only needs to include DOFs 4, 5, and 6 due to the fact that DOFs 1, 2, and 3 and DOFs 7, 8, and 9 are constrained. The elements in the global stiffness matrix is the result of adding the elements in the global stiffness matrices of Elements 1 and 2 that are contributive to the stiffness corresponding to DOFs 4,5, and 6, as is shown in Equation 12.

$$[K]=\begin{bmatrix} \frac{12EI}{L^3}+\frac{EA}{L} & & \frac{6EI}{L^2} \\ & \frac{EA}{L}+\frac{12EI}{L^3} & \frac{6EI}{L^2} \\ \frac{6EI}{L^2} & \frac{6EI}{L^2} & \frac{8EI}{L} \end{bmatrix} \tag{11}$$

7.1.6. Load assembly

The nodal load vector in the global coordinate system corresponding to DOFs 4, 5, and 6 is as shown in Equation 13.

$$[F] = [Q_1 \quad 0 \quad 0]^T \tag{12}$$

All the non-nodal loads need to be transformed to equivalent nodal loads according to the method introduced in structural analysis [47]. The equivalent nodal loads in the global coordinate system of Elements 1 and 2 are as shown in Equations 14 and 15, respectively.

$$[F_0^1] = [T_1]^T [0 \quad Q/2 \quad QL/8 \quad 0 \quad Q/2 \quad -QL/8]^T = [-Q/2 \quad 0 \quad QL/8 \quad -Q/2 \quad 0 \quad -QL/8]^T \tag{13}$$

$$[F_0^2] = \left[0 \quad pL/2 \quad pL^2/12 \quad 0 \quad pL/2 \quad -pL^2/12\right]^T \tag{14}$$

Then the global load vector for the matrix stiffness method in this case is as shown in Equation 16, which is the nodal load minus equivalent load contributive to the loading at DOFs, 4, 5, and 6.

$$[P] = [Q_1 + Q/2 - pL/2 \quad QL/8 + pL^2/12]^T \tag{15}$$

7.1.7. Problem solving and internal force and reaction calculation

With the global stiffness matrix and the load assembled for the active degree of freedoms, the displacement can be solved easily by dividing the load vector by the stiffness matrix or multiplying the inverse of the stiffness matrix with the load vector, as is shown in Equation 17. Then the element internal forces can be calculated by multiplying the element displacement vector with the element stiffness matrix plus the equivalent nodal load as developed in Equation 15, and then transformed to the forces in the local element coordinate system. The reaction forces are sum of element forces in the global coordinate system of elements connected by that support.

$$[\delta] = [K]^{-1}[P] \tag{16}$$

In the example described in **7.1.5**, the displacement vector solved by Equation 17 can be expressed in detail with the displacements at Node 2, as is shown in Equation 18.

$$[\delta] = [\delta_4 \quad \delta_5 \quad \delta_6]^{\mathrm{T}} \tag{17}$$

Then the element forces can be calculated by Equations 19 and 20, and transformed to local element forces by Equations 21 and 22, respectively.

$$\begin{Bmatrix} F_{\mathrm{X}}^{11} \\ F_{\mathrm{Y}}^{11} \\ M_{\mathrm{Z}}^{11} \\ F_{\mathrm{X}}^{21} \\ F_{\mathrm{Y}}^{21} \\ M_{\mathrm{Z}}^{21} \end{Bmatrix} = [k_{\mathrm{G}}^{1}] \begin{Bmatrix} 0 \\ 0 \\ 0 \\ \delta_4 \\ \delta_5 \\ \delta_6 \end{Bmatrix} + [F_0^1] \tag{18}$$

$$\begin{Bmatrix} F_{\mathrm{X}}^{22} \\ F_{\mathrm{Y}}^{22} \\ M_{\mathrm{Z}}^{22} \\ F_{\mathrm{X}}^{32} \\ F_{\mathrm{Y}}^{32} \\ M_{\mathrm{Z}}^{32} \end{Bmatrix} = [k_{\mathrm{G}}^{2}] \begin{Bmatrix} \delta_4 \\ \delta_5 \\ \delta_6 \\ 0 \\ 0 \\ 0 \end{Bmatrix} + [F_0^2] \tag{19}$$

$$\begin{Bmatrix} F_{\mathrm{x}}^{11} \\ F_{\mathrm{y}}^{11} \\ M_{\mathrm{z}}^{11} \\ F_{\mathrm{x}}^{21} \\ F_{\mathrm{y}}^{21} \\ M_{\mathrm{z}}^{21} \end{Bmatrix} = [T_1] \begin{Bmatrix} F_{\mathrm{X}}^{11} \\ F_{\mathrm{Y}}^{11} \\ M_{\mathrm{Z}}^{11} \\ F_{\mathrm{X}}^{21} \\ F_{\mathrm{Y}}^{21} \\ M_{\mathrm{Z}}^{21} \end{Bmatrix} \tag{20}$$

$$\begin{Bmatrix} F_{\mathrm{x}}^{22} \\ F_{\mathrm{y}}^{22} \\ M_{\mathrm{z}}^{22} \\ F_{\mathrm{x}}^{32} \\ F_{\mathrm{y}}^{32} \\ M_{\mathrm{z}}^{32} \end{Bmatrix} = [T_2] \begin{Bmatrix} F_{\mathrm{X}}^{22} \\ F_{\mathrm{Y}}^{22} \\ M_{\mathrm{Z}}^{22} \\ F_{\mathrm{X}}^{32} \\ F_{\mathrm{Y}}^{32} \\ M_{\mathrm{Z}}^{32} \end{Bmatrix} \tag{21}$$

Then the reaction forces at Nodes 1 and 3 are the element internal forces in the global coordinate system, as are shown in Equations 23 and 24.

$$\begin{Bmatrix} R_X^1 \\ R_Y^1 \\ R_Z^1 \end{Bmatrix} = \begin{Bmatrix} F_X^{11} \\ F_Y^{11} \\ M_Z^{11} \end{Bmatrix} \tag{22}$$

$$\begin{Bmatrix} R_X^3 \\ R_Y^3 \\ R_Z^3 \end{Bmatrix} = \begin{Bmatrix} F_X^{32} \\ F_Y^{32} \\ M_Z^{32} \end{Bmatrix} \tag{23}$$

7.2. Program Development and Validation

7.2.1. Program development

The computer program for matrix stiffness method of structural analysis. The program includes the following modules:

1. Input
2. Generation of element stiffness matrix in local coordinates
3. Coordinate transformation
4. Assembly of global stiffness matrix
5. Assembly of global load vectors
6. Solving stiffness equations
7. Calculating element forces
8. Calculating support reactions
9. Organized output report (geometry, loads, deformations, forces, reactions, etc.)

The MATLAB scripts as attached in APPENDIX. SCRIPTS are the developed computer code. The input data include the number of elements (Nelems), number of nodes (Nndoes), element modulus of elasticity (ElemE), element area (ElemArea), element moment of inertia (ElemInertia), element length (ElemLength), element coordinate system angle with respect to global coordinate system (ElemAlpha), element node number (ElemNodes), boundary conditions (NOdeMov) with

1 indicating restrained and 0 free, nodal load (NodeLoads), and element load (ElemLoads). The script "main.m" contains the input information and the implementation of the program; "fillFrameGdof.m" is the assembly of degree of freedom based on the boundary condition, the outcome of this module is a matrix demonstrating the effective DOF number of each DOF at each node (DOFNum) and the total number of DOFs (Ndof); "assmblFrameGS.m" assembles the global stiffness matrix of the bridge structure; "prepareFrameLoadVec.m" is the preparation of loading conditions for the problem solution, generating the nodal load vector (P) and the equivalent nodal load vector (Pf); The global displacement is obtained by dividing the load vector by the global stiffness matrix; "elemForcesFrame.m" calculates the element forces as mentioned in 7.1.7; "supportR.m" is for the calculation of reaction forces.

7.2.2. Program validation

The composite rigid frame bridge is modelled using the computer program developed in this section. The bridge is discretized into frame elements of 1m in element length, ending up with 464 elements and 465 nodes. For the elements of concrete girder with non-uniform cross-section area and moment of inertia, the computer program takes the average of the values at the element ends. The dead load case is used for validation. All the loads are applied onto the element nodes directly for simplicity.

To validate the computer program developed above, this section calculates and compares the bending moments of several cross sections of the bridge girder under dead load using the finite element method and the computer program as is tabulated in Table 22. The last row lists the relative difference of the bending moments by computer program compared with that from the finite element method. It shows that the bending moments of the bridge girder calculated from the two methods are very close to each other with a relative difference below 15%, validating the

effectiveness of the computer program. In future work, the computer program will be used for advanced analysis of the bridge, e.g., nonlinear analysis, structural optimization. etc., considering the various analysis tools available in MATLAB Toolbox.

Table 22. Comparison of Bending Moments from Finite Element Analysis and Computer Program (kN.m)

Method	¼ side span	½ side span	¾ side span	Left pier	Right pier	¼ midspan	Intersection	Center of midspan
Finite element method	51422	-79889	-426066	-960580	-1117568	-103981	-23756	96372
Computer program	54803	-78683	-489064	-1121069	-1155164	-120098	-27806	88765
Relative difference	7%	-2%	15%	17%	3%	15%	17%	-8%

8. CONCLUSIONS AND FUTURE WORK

This thesis optimizes the structural parameters of composite rigid frame bridge based on the results of parametric analysis and develops the computer program for matrix stiffness method of structural analysis using MATLAB. This work provides structural engineers with suggestions with respect to the structural design and analysis of composite rigid frame bridge. The computer program developed in this thesis lays a foundation for further advanced structural analysis and optimization using the powerful toolboxes included in MATLAB. The conclusions of this thesis study include:

1) This study developed the finite element model of the composite rigid frame bridge based on beam elements using the finite element software MIDAS CIVIL 2010.
2) Parametric analysis on steel span ratio shows that a large ratio or a small ratio leads to large tension stress on the concrete girders. A steel span ratio of 0.55 has the minimum bending strain energy, uniform bending moment distribution, and generally lower stress level on concrete girder, though the steel girder has relatively high stress level that is acceptable for structural design.
3) A composite rigid frame bridge with a large bottom girder curve order has a relatively large stress at the ¼ side span, and a small curve order increases the weight of bridge and thus the tension stress of girder at the inner supports. A curve order of 1.3 has a low value to bending strain energy and a minimum bending moment at the intersection.
4) A large midspan depth-to-span ratio brings high stress level at ¼ span, and a small ratio high stress on the concrete girder at the inner supports. An optimization based on bending strain energy ends up with an optimal midspan depth-to-span ratio of 1/32.

5) Different from the midspan depth-to-span ratio, a high stress on the concrete girder at the inner supports happens when the support depth-to-span ratio has a relatively large magnitude. A bridge with small support depth-to-span ratio has a large girder weight and can't make full use of the concrete girder's capability. A ratio of 1/16 or 1/17 has the minimum bending strain energy and a uniform bending moment distribution.
6) This thesis study also developed the computer program for structural analysis using the matrix stiffness method with MATLAB. A comparison with the results from finite element analysis validates the effectiveness of the computer program.

Future work will be remaining to analyze and optimize the composite rigid frame bridge using the developed computer program and the advanced analyzing capabilities of MATLAB toolbox.

REFERENCES

1. Mei, G., *Stability Analysis of the Continuous Rigid Frame Bridge with High Pier and Large Span [J]*. Journal of Xi'an Highway Univerisity 1999. **3**: p. 007.
2. FENG, P.-c., et al., *Analysis of Accident of Bursting Crack in Bottom Slab of a Continuous Rigid-Frame Bridge [J]*. World Bridges, 2006. **1**: p. 66-69.
3. Zhouhong, Z., et al., *Analysis of dynamic characteristics of a large-span prestressed concrete continuous rigid frame bridge.* Earthquark Engineering and Engineering Vibration-Chinese Edition, 2004. **24**(3): p. 98-104.
4. XIANG, Y.-q., et al., *Study of static and dynamic behavior of T-shape rigid frame bridge reinforced by prestressed external tendon [J]*. China Journal of Highway and Transport, 2004. **1**: p. 009.
5. Peng-cheng, F., *Study of Key Technical Issues on Design of Continuous Rigid-Frame Bridge [J]*. Bridge Construction, 2009. **6**: p. 011.
6. Kwak, H.-G. and Y.-J. Seo, *Long-term behavior of composite girder bridges.* Computers & Structures, 2000. **74**(5): p. 583-599.
7. Adeli, H. and J. Zhang, *Fully nonlinear analysis of composite girder cable-stayed bridges.* Computers & structures, 1995. **54**(2): p. 267-277.
8. Li-zhong, W., *Design of the Rotational Struction of Highway T-Shape Rigid Frame Brige Constructed with the Method of Slewing [J]*. Journal of Railway Engineering Society, 2006. **9**: p. 41-43.
9. Aashto, L., *Bridge design specifications*. 1998, American Association of State Highway and Transportation Officials, Washington, DC.
10. Brockenbrough, R.L. and F.S. Merritt, *Structural steel designer's handbook*. 1999: McGraw-Hill New York.
11. Heins, C., *Box girder bridge design-State of the art.* Engineering Journal, 1978. **15**(4).
12. Lin, K.-Y. and D.M. Frangopol, *Reliability-based optimum design of reinforced concrete girders.* Structural safety, 1996. **18**(2-3): p. 239-258.
13. Wilde, D.J., *Globally optimal design.* 1978.
14. Lute, V., A. Upadhyay, and K.K. Singh, *Computationally efficient analysis of cable-stayed bridge for GA-based optimization.* Engineering Applications of Artificial Intelligence, 2009. **22**(4): p. 750-758.
15. Cheng, J., *Optimum design of steel truss arch bridges using a hybrid genetic algorithm.* Journal of Constructional Steel Research, 2010. **66**(8): p. 1011-1017.
16. Hassan, M., *Optimization of stay cables in cable-stayed bridges using finite element, genetic algorithm, and B-spline combined technique.* Engineering Structures, 2013. **49**: p. 643-654.
17. Martins, A., L. Simões, and J. Negrão, *Optimization of cable forces on concrete cable-stayed bridges including geometrical nonlinearities.* Computers & Structures, 2015. **155**: p. 18-27.
18. Baldomir, A. and S. Hernández, *Cable optimization of a long span cable stayed bridge in La Coruña (Spain).* Computer Aided Optimum Design in Engineering XI, 2009. **106**: p. 107.
19. Kusano, I., et al., *Reliability based design optimization of long-span bridges considering flutter.* Journal of Wind Engineering and Industrial Aerodynamics, 2014. **135**: p. 149-162.

20. Martí, J.V., et al., *Design of prestressed concrete precast road bridges with hybrid simulated annealing.* Engineering Structures, 2013. **48**: p. 342-352.
21. Martínez, F.J., et al., *Design of tall bridge piers by ant colony optimization.* Engineering Structures, 2011. **33**(8): p. 2320-2329.
22. Frangopol, D.M., *Structural optimization using reliability concepts.* Journal of Structural Engineering, 1985. **111**(11): p. 2288-2301.
23. Nieto, F., S. Hernández, and J. Jurado, *Optimum design of long-span suspension bridges considering aeroelastic and kinematic constraints.* Structural and Multidisciplinary Optimization, 2009. **39**(2): p. 133-151.
24. Yang, R., *Shape design sensitivity analysis with frequency response.* Computers & Structures, 1989. **33**(4): p. 1089-1093.
25. Tan, R.C., *Some acceleration methods for iterative computer of derivatives of eigenvalues and eigenvectors.* International journal for numerical methods in engineering, 1989. **28**(7): p. 1505-1519.
26. Jurado, J.Á., et al., *Efficient cable arrangement in cable stayed bridges based on sensitivity analysis of aeroelastic behaviour.* Advances in Engineering Software, 2008. **39**(9): p. 757-763.
27. Mosquera, A., S. Hernández, and J. Jurado. *Analytical sensitivity analysis of aeroelastic performance of suspension bridges under construction*. in *11th International conference on wind engineering, Lubbock, Texas, USA*. 2003.
28. Jurado, J. and S. Hernandez, *Sensitivity analysis of bridge flutter with respect to mechanical parameters of the deck.* Structural and Multidisciplinary Optimization, 2004. **27**(4): p. 272-283.
29. Nieto, F., S. Hernandez, and J. Jurado, *Distributed computing for design optimization of the messina bridge considering aeroelastic constraints.* Journal of Wind Engineering, 2006. **108**: p. 757-760.
30. Chen, D., et al., *Determination of initial cable forces in prestressed concrete cable-stayed bridges for given design deck profiles using the force equilibrium method.* Computers & Structures, 2000. **74**(1): p. 1-9.
31. Sung, Y.-C., D.-W. Chang, and E.-H. Teo, *Optimum post-tensioning cable forces of Mau-Lo Hsi cable-stayed bridge.* Engineering Structures, 2006. **28**(10): p. 1407-1417.
32. Furukawa, K., et al. *Optimization of Cable Prestresses of Cable Stayed Bridges Based on Minimum Strain Energy Criterion*. ASCE.
33. Kaveh, A., et al., *Structural topology optimization using ant colony methodology.* Engineering Structures, 2008. **30**(9): p. 2559-2565.
34. Furukawa, K., et al. *Studies on optimization of cable prestressing for cable-stayed bridges*. in *Proceedings of International Conference on Cable-stayed Bridges, Bangkok*. 1987.
35. Lee, T.-Y., Y.-H. Kim, and S.-W. Kang, *Optimization of tensioning strategy for asymmetric cable-stayed bridge and its effect on construction process.* Structural and Multidisciplinary Optimization, 2008. **35**(6): p. 623-629.
36. Negrão, J. and L. Simões, *Optimization of cable-stayed bridges with three-dimensional modelling.* Computers & Structures, 1997. **64**(1-4): p. 741-758.
37. Everitt, B., *Cambridge dictionary of statistics*. 1998: Cambridge University Press.
38. Yang, Y.X. and L. Sun. *Spatial Analysis of Continuous Rigid Frame High Pier under Completed Bridge State*. in *Advanced Materials Research*. 2011. Trans Tech Publ.

39. Zhang, W.H., Y.T. Zhang, and G.Q. Li. *Evolutionary Structural Topology Optimization for Cantilever Construction of Continuous Rigid-Frame Bridge*. in *Applied Mechanics and Materials*. 2011. Trans Tech Publ.
40. Zhang, Y.B. and D.P. Liu. *Research on Setting of Pre-Camber of Long-Span Continuous Rigid Frame Bridge with High Piers*. in *Advanced Materials Research*. 2011. Trans Tech Publ.
41. Zheng, H.B., et al. *Parameter Sensitivity Analysis of Vertical Deflection for Long-Span Continuous Rigid-Frame Bridge*. in *Advanced Materials Research*. 2011. Trans Tech Publ.
42. Shi, Y., et al. *Spatial analysis of vehicle-bridge coupled vibration response between curved continuous rigid-frame bridge and motor vehicle*. in *Applied Mechanics and Materials*. 2012. Trans Tech Publ.
43. Wang, R.X., et al. *Study on the Influence of Beam Rigidity on Continuous Rigid Frame Bridge with Moving Vehicle*. in *Advanced Materials Research*. 2012. Trans Tech Publ.
44. Xue, X.W., H. Yuan, and S.Q. Li. *Study on Optimizing Design of Structural Rigidity of Super-Large Span Continuous Rigid Frame Bridge Using ANSYS*. in *Advanced Materials Research*. 2012. Trans Tech Publ.
45. Yang, Y.X. *Analysis of Stress Measuring and Testing of Continuous Rigid Frame Bridge*. in *Advanced Materials Research*. 2012. Trans Tech Publ.
46. McGuire, W., R.H. Gallagher, and R.D. Ziemian, *Matrix structural analysis*. 2000.
47. Nayfeh, A.H. and P.F. Pai, *Linear and nonlinear structural mechanics*. 2008: John Wiley & Sons.

APPENDIX. SCRIPTS

main.m

```
% ~~~~~~~~~~~~~~~~~~~~~~~~~~~~~~~~~~~~~~~~~~~~~~~~~~~~
% This is the main script of this program.
% It contains the lines for information input and
% that for the execution of other scripts
% taking the information as input.
% By Yanmei Xie, 2016
% ~~~~~~~~~~~~~~~~~~~~~~~~~~~~~~~~~~~~~~~~~~~~~~~~~~~~
clear all
%% Input data, Unit: N, m
Nelems = 464;                   % Number of elements
Nnodes = 465;                   % Total number of nodes in system
ElemE = zeros(Nelems,1);        % Element modulus of elasticity
ElemArea = zeros(Nelems,1);     % Element area
ElemInertia = zeros(Nelems,1);  % Element momnet of inertia
ElemLength = zeros(Nelems,1);   % Element length
ElemAlpha = zeros(Nelems,1);    % Element angle vs global coord system
ElemNodes = zeros(Nelems,2);    % Element node numbers
NodeMov = zeros(Nnodes,3);      % Node movements 1: restrained 0: free
NodeLoads = zeros(Nnodes,3);    % Node loads in the global coord system
ElemLoads = zeros(Nelems,6);    % Elem loads in the local element coord system
%%
% DOFNum matrix and number of effective DOF
[DOFNum, Ndof] = fillFrameGdof(Nnodes, NodeMov);
% Global stiffness matrix
[S] = assmblFrameGS(ElemE,ElemArea,ElemInertia,ElemLength,ElemAlpha,Nelems,Ndof,ElemNodes,DOFNum);
% Global load vector: nodal load and equivalent nodal load
[P, Pf] = prepareFrameLoadVec(NodeLoads,ElemLoads,ElemAlpha,Nelems,Nnodes,Ndof,DOFNum);
% Solving the global displacement
Gdelta = S \ (P-Pf);
% element forces in local coordinate system
elemMV =
elemForcesFrame(Nelems,ElemNodes,DOFNum,ElemLoads,ElemArea,ElemE,ElemInertia,ElemLength,ElemAlpha
,Gdelta);
% support reactions in global coordinate system
supportR = suppReactionsFrame(Nelems,Nnodes,ElemNodes,ElemAlpha,DOFNum,elemMV);
```

fillFrameGdof.m

```
function [DOFNum, Ndof] = fillFrameGdof(Nnodes, NodeMov)
% ~~~~~~~~~~~~~~~~~~~~~~~~~~~~~~~~~~~~~~~~~~~~~~~~~~~~
% This script fills the array DOFNum(Nnodes*3)
% for frame structure
% with appropriate global DOF number.
% It also determines the total number of DOFs
% in the problem
% By Yanmei Xie, 2016
%~~~~~~~~~~~~~~~~~~~~~~~~~~~~~~~~~~~~~~~~~~~~~~~~~~~~
% initialize an empty matrix of the right order Nnodes*3.
% 3 columns are needed with two for translations and
% the other for rotations. Other element types may require
% a different number of columns
NumDofNode = 3;
DOFNum = zeros(Nnodes,NumDofNode);
%% initialize the DOF counter for valid global DOFs
DOFCounter = 0;
% loop over all nodes
for Inode = 1:Nnodes
        % loop over each DOF
        for Idof = 1:NumDofNode
                if(NodeMov(Inode,Idof)==0)
                % increase totla DOF number for each new DOF
                DOFCounter = DOFCounter + 1;
                DOFNum(Inode,Idof) = DOFCounter;
                else
                % enter a zero for restrained DOFs
                DOFNum(Inode,Idof) = 0;
                end
        end
end
% store the totoal number of DOFs for future use
Ndof = DOFCounter;
end
```

getFrameElemK.m

```
function [K] = getFrameElemK(E,A,I,L)
% ~~~~~~~~~~~~~~~~~~~~~~~~~~~~~~~~~~~~~~~~~~~~~~~~~~~~
% This function generates the stiffness matrix
% for a frame element DIRECTLY
% E: Modulus of elasticity
% A: Area
% I: Moment of inertia
% L: Element length
% By Yanmei Xie, 2016
%~~~~~~~~~~~~~~~~~~~~~~~~~~~~~~~~~~~~~~~~~~~~~~~~~~~~
K = [   E*A/L,          0,              0,              -E*A/L      0               0;...
        0,              12*E*I/L^3,     6*E*I/L^2,      0,          -12*E*I/L^3,    6*E*I/L^2;...
        0,              6*E*I/L^2       4*E*I/L,        0,          -6*E*I/L^2,     2*E*I/L;...
        -E*A/L,         0,              0,              E*A/L,      0,              0;...
        0,              -12*E*I/L^3,    -6*E*I/L^2,     0,          12*E*I/L^3,     -6*E*I/L^2;...
        0,              6*E*I/L^2,      2*E*I/L,        0,          -6*E*I/L^2,     4*E*I/L
        ];
end
```

coordTransMatrix.m

```
function [T] = coordTransMatrix(beta)
% ~~~~~~~~~~~~~~~~~~~~~~~~~~~~~~~~~~~~~~~~~~~~~~~~~~~~~~~~~~~~~~~~~~~~~~~~~~~~
% This function generates the coordinate transforming matrix T
% for a frame element DIRECTLY
% beta: angle between local axis and global axis in radians
% By Yanmei Xie, 2016
%~~~~~~~~~~~~~~~~~~~~~~~~~~~~~~~~~~~~~~~~~~~~~~~~~~~~~~~~~~~~~~~~~~~~~~~~~~~~~
c = cos(beta);
s = sin(beta);
T = [   c,      s,      0,      0,      0,      0;...
        -s,     c,      0,      0,      0,      0;...
        0,      0,      1,      0,      0,      0;...
        0,      0,      0,      c,      s,      0;...
        0,      0,      0,      -s,     c,      0;...
        0,      0,      0,      0,      0,      1       ];
end
```

assmblFrameGS.m

```
function [S] = assmblFrameGS(ElemE,ElemArea,ElemInertia,ElemLength,ElemAlpha,Nelems,Ndof,ElemNodes,DOFNum)
% ~~~~~~~~~~~~~~~~~~~~~~~~~~~~~~~~~~~~~~~~~~~~~~~~~~~~~~~~~~~~
% This script assembles the global stiffness matrix
% for the frame problems.
% By Yanmei Xie, 2016
%~~~~~~~~~~~~~~~~~~~~~~~~~~~~~~~~~~~~~~~~~~~~~~~~~~~~~~~~~~~~~~
%% Initialize an empty square matirx of Ndof*Ndof
S = zeros(Ndof,Ndof);
%% Loop over all elements
for Ielem = 1:Nelems,
	%% get the local element stiffness matrix and transform it into the global coord system
	K = getFrameElemK(ElemE(Ielem),ElemArea(Ielem),ElemInertia(Ielem),ElemLength(Ielem));
	T = coordTransMatrix(ElemAlpha(Ielem));
	K_bar = T'*K*T;
	%% get end node numbers for the element Ielem
	NodeNum1 = ElemNodes(Ielem,1);
	NodeNum2 = ElemNodes(Ielem,2);
	%% find the global numbering of DOFs for this element and store them
	% in a vector
	NumDof = zeros(6,1);
	NumDof(1) = DOFNum(NodeNum1,1);
	NumDof(2) = DOFNum(NodeNum1,2);
	NumDof(3) = DOFNum(NodeNum1,3);
	NumDof(4) = DOFNum(NodeNum2,1);
	NumDof(5) = DOFNum(NodeNum2,2);
	NumDof(6) = DOFNum(NodeNum2,3);
	%% build a 2-column array that stores the non-zero NumDof in the first
	% column and its index (1~6) in the second column
	tempArray = zeros(6,2);
	tempIndex = 0;
	for Indof = 1:6
		if NumDof(Indof) ~= 0
			tempIndex = tempIndex + 1;
			tempArray(tempIndex,1) = NumDof(Indof);
			tempArray(tempIndex,2) = Indof;
		else
			tempArray(tempIndex+1,:) = [];
		end
	end
	%% fill in upper triangular terms of [K] in [S] ONLY for FREE DOFS
	for i = 1:length(tempArray)
		for j = i:length(tempArray)
			S(tempArray(i,1),tempArray(j,1)) = S(tempArray(i,1),tempArray(j,1))...
			+ K_bar(tempArray(i,2),tempArray(j,2));
		end
	end
end
%% fill in the symmetric terms
for Irow = 1:Ndof
	for Icol = 1:Irow-1
		S(Irow,Icol) = S(Icol,Irow);
	end
end
end
```

prepareFrameLoadVec.m

```
function [P, Pf] = prepareFrameLoadVec(NodeLoads,ElemLoads,ElemAlpha,Nelems,Nnodes,Ndof,DOFNum)
% ~~~~~~~~~~~~~~~~~~~~~~~~~~~~~~~~~~~~~~~~~~~~~~~~~~~~~~~~~~~~
% This script prepares the load vector [14] and {Pf}
% of order Ndof*1 using the input information stored
% in NodeLoads and ElemLoads
% By Yanmei Xie, 2016
%~~~~~~~~~~~~~~~~~~~~~~~~~~~~~~~~~~~~~~~~~~~~~~~~~~~~~~~~~~~~
%% initialize two empty vectors of the order Ndof*1
P = zeros(Ndof,1);
Pf = zeros(Ndof,1);
%% transform the equivalent element loads to the global coord system
ElemLoadsGlobal = zeros(size(ElemLoads,1),size(ElemLoads,2));
for Ielem = 1:Nelems
	T = coordTransMatrix(ElemAlpha(Ielem));
	ElemLoadsGlobal(Ielem,:) = (T' * ElemLoads(Ielem,:)')';
end
%% first deal with nodal loads
for Inode = 1:Nnodes
	for Idof = 1:size(DOFNum,2)
		if(DOFNum(Inode,Idof) ~= 0)
			P(DOFNum(Inode,Idof)) = P(DOFNum(Inode,Idof)) + NodeLoads(Inode,Idof);
		end
	end
end
%% now deal with element loads
for Inode = 1:Nnodes
	for Idof = 1:size(DOFNum,2)
		if DOFNum(Inode,Idof) ~= 0
			% the Pf at (Inode,Idof)) is composed of two parts
			% 1. Element Inode at DOF Idof
			% 2. Element Inode-1 at DOF Idof+size(DOFNum,2)
			if Inode <= Nnodes-1
				Pf(DOFNum(Inode,Idof)) = ...
				Pf(DOFNum(Inode,Idof)) + ElemLoadsGlobal(Inode,Idof);
			end
			if Inode >= 2
				Pf(DOFNum(Inode,Idof)) = ...
				Pf(DOFNum(Inode,Idof))+ ElemLoadsGlobal(Inode-1,Idof+size(DOFNum,2));
			end
		end
	end
end
end
```

elemForcesFrame.m

```
function elemMV = elemForcesFrame(Nelems,ElemNodes,DOFNum,ElemLoads,ElemArea,ElemE,ElemInertia,ElemLength,ElemAlpha,Gdelta)
%~~~~~~~~~~~~~~~~~~~~~~~~~~~~~~~~~~~~~~~~~~~~~~~~~~~~~~~~
% This script calculates element forces
% after extracting local data.
% By Yanmei Xie, 2016
%~~~~~~~~~~~~~~~~~~~~~~~~~~~~~~~~~~~~~~~~~~~~~~~~~~~~~~~~
%% Initialize an empty matrix
elemMV = zeros(Nelems,6);
%% Loop over all elements
for Ielem = 1:Nelems
        % local element displacement at nodes in GLOBAL COORD SYSTEM!!!
        Ldelta = zeros(6,1);
        % local element stiffness matrix
        K = getFrameElemK(ElemE(Ielem),ElemArea(Ielem),ElemInertia(Ielem),ElemLength(Ielem));
        % local element DOF
        Ldof = 0;
        for Inode = 1:2
                NodeNum = ElemNodes(Ielem,Inode);
                for Idof = 1:size(DOFNum,2)
                        Ldof = Ldof + 1;
                        Gdof = DOFNum(NodeNum,Idof);
                        if Gdof ~= 0
                                Ldelta(Ldof) = Gdelta(Gdof);
                        else
                                Ldelta(Ldof) = 0;
                        end
                end
        end
        % calculate local element forces
        T = coordTransMatrix(ElemAlpha(Ielem));
        LP = K * (T*Ldelta) + ElemLoads(Ielem,:)';
        elemMV(Ielem,:) = LP';
end
end
```

suppReactionsFrame.m

```
function supportR = suppReactionsFrame(Nelems,Nnodes,ElemNodes,ElemAlpha,DOFNum,elemMV)
%~~~~~~~~~~~~~~~~~~~~~~~~~~~~~~~~~~~~~~~~~~~~~~~~~~~~~~~~~~~~
% This script calculates support reaction
% element forces.
% By Yanmei Xie, 2016
%~~~~~~~~~~~~~~~~~~~~~~~~~~~~~~~~~~~~~~~~~~~~~~~~~~~~~~~~~~~~
%% initialize an empty matrix
supportR = zeros(Nnodes,3);
%% loop over all elements
for Ielem = 1:Nelems
        % local element DOF
        Ldof = 0;
        for Inode = 1:2
                NodeNum = ElemNodes(Ielem,Inode);
                for Idof = 1:size(DOFNum,2)
                        Ldof = Ldof + 1;
                        if (DOFNum(NodeNum,Idof) == 0)
                                T = coordTransMatrix(ElemAlpha(Ielem));
                                % transform the elment force into the global coord system
                                % so that the final support reactions are in the global coord system
                                elemMVglobal = T'*elemMV(Ielem,:)';
                                supportR(NodeNum,Idof) = supportR(NodeNum,Idof) + elemMVglobal(Ldof);
                        end
                end
        end
end
end
```